

Nearest neighbor synthesis of CNOT circuits on general quantum architectures

Xinyu Chen,* Mingqiang Zhu,* Xueyun Cheng,[†] and Zhijin Guan

School of Information Science and Technology, Nantong University, Nantong 226019, China

Shiguang Feng

School of Computer Science and Engineering, Sun Yat-sen University, Guangzhou 510006, China

Pengcheng Zhu

Department of Artificial Intelligence, Suqian University, Suqian, 223800, China

(Dated: June 8, 2025)

NISQ devices have inherent limitations in terms of connectivity and hardware noise. The synthesis of CNOT circuits considers the physical constraints and transforms quantum algorithms into low-level quantum circuits that can execute on physical chips correctly. In the current trend, quantum chip architectures without Hamiltonian paths are gradually replacing architectures with Hamiltonian paths due to their scalability and low-noise characteristics. To this end, this paper addresses the nearest neighbor synthesis of CNOT circuits in the architectures with and without Hamiltonian paths, aiming to enhance the fidelity of the circuits after execution. Firstly, a key-qubit priority mapping model for general quantum architectures is proposed. Secondly, the initial mapping is further improved by using tabu search to reduce the number of CNOT gates after circuit synthesis and enhance its fidelity. Finally, the noise-aware CNOT circuit nearest neighbor synthesis algorithm for the general architecture is proposed based on the key-qubit priority mapping model. The algorithm is demonstrated on several popular cloud quantum computing platforms and simulators, showing that it effectively optimizes the fidelity of CNOT circuits compared with mainstream methods. Moreover, the method can be extended to more general circuits, thereby improving the overall performance of quantum computing on NISQ devices.

I. INTRODUCTION

Quantum computing is a new computing paradigm that follows the laws of quantum mechanics to perform complex tasks. It can provide up to exponential speedups over classical algorithms in integer factorization [1, 2], database search [3], quantum many-body simulation [4], *etc.* Moreover, quantum computing has potential applications in cryptography [5], chemistry [6, 7], artificial intelligence [8, 9] and other areas. In recent years, quantum computing has entered the era of Noisy Intermediate-Scale Quantum (NISQ), which supports quantum computing with tens to hundreds of qubits. However, NISQ devices are limited in their ability to apply only a few elementary quantum gates due to the presence of noise. Among these gates, the CNOT gate is widely employed in quantum computing as it can be combined with other single-qubit gates to construct a universal gate library [10]. The circuits composed of CNOT gates cannot be executed directly since the nearest neighbor (NN) constraint and error rate of NISQ devices are affected by the physical architecture. Instead, these circuits must be further transformed into a suitable form that can be implemented on actual quantum hardware.

Currently, there are two main methods to obtain a quantum circuit that satisfies the NN constraint. The first method involves inserting SWAP gates in front of

quantum gates that do not satisfy the NN constraint after the initial mapping [11–13]. This ensures the connection of non-nearest neighbor gates on physical qubits. Since a SWAP gate can be decomposed into three CNOT gates, this method necessitates the insertion of additional CNOT gates. Consequently, the depth of the final circuit increases, raising the probability of errors in the circuit. The other approaches focus on researching the synthesis of quantum circuits directly under NN constraints. Quantum circuit synthesis enables the transformation of a matrix representing a quantum algorithm into a quantum circuit supporting a specific library of gates [14–19]. The synthesis method that generates a circuit containing only CNOT gates is CNOT circuit synthesis. The resulting CNOT circuits do not necessarily satisfy the NN constraint of the physical architecture and cannot be executed on real quantum computing devices. To address this issue, the CNOT circuit NN synthesis method that transforms the Boolean matrix into a CNOT circuit satisfying the NN constraint of the physical architecture was proposed to solve this problem [20–28].

Several researchers have dedicated their efforts to the synthesis of quantum circuits. In [20], CNOT circuits were represented as Boolean matrices, and a CNOT circuit synthesis algorithm based on Gaussian elimination and LU decomposition was proposed. However, the NN constraints between control and target qubits of CNOT gates were not considered. A linear NN Gaussian elimination method was proposed in [21], which shared a similar structure to the Gaussian elimination method. But the row operations must be performed between adjacent

* Xinyu Chen and Mingqiang Zhu contributed equally to this work.

[†] chen.xy@ntu.edu.cn

rows, and this method is only applicable to the NN synthesis problem of CNOT circuits in a one-dimensional (1D) structure. In [22] and [23], the NN synthesis methods for CNOT circuits in a two-dimensional (2D) structure were proposed, relying on Steiner trees to determine the NN interaction paths on a 2D grid. A similar strategy was proposed in [24]. These methods all use Steiner trees to determine the interaction paths that satisfy the NN constraint. In contrast to the traditional Gaussian elimination, they do not completely rely on the main diagonal elements in the elimination process, but they use the neighboring elements with value 1 in the Steiner tree to achieve the row elimination. In [25], a new algorithm for CNOT circuit synthesis based on corrected sub-decoding was proposed to solve the problem of synthesizing CNOT circuits with fully connected topologies as well as quantum devices with topologically constrained structures. The authors in [26] aimed to reduce the effect of noise on CNOT circuit synthesis by reducing the number of CNOT gates and circuit depth, while minimizing the errors generated during the synthesis process.

Some of the above studies focus on CNOT circuit synthesis on quantum architectures with Hamiltonian paths. A Hamiltonian path in a graph is defined as a path that visits each vertex in the graph exactly once, showcasing a potential route for optimal quantum gates arrangement. However, with the development of NISQ devices, architectures without Hamiltonian paths are gradually replacing those with Hamiltonian paths because of their excellent scalability and high fault tolerance. Consequently, the CNOT circuit synthesis methods designed for architectures with Hamiltonian paths cannot be directly applied to architectures without Hamiltonian paths. Various solutions have been proposed to address this challenge. Although the core method in [23] originally targeted architectures with Hamiltonian paths, its recursive extension explicitly addresses this limitation by enabling synthesis on architectures without Hamiltonian paths. Meanwhile, both [27] and [28] presented ROWCOL methods for implementing NN synthesis of CNOT circuits on arbitrary architectures. These methods prioritize the elimination of certain qubits and subsequently disconnect them. This allows finding suboptimal Hamiltonian paths in architectures where no Hamiltonian paths exist. Through this process, the size of the problem is gradually reduced. Another approach is to use matrix decomposition techniques [29] to represent the quantum algorithm as a quantum circuit. The circuit is then mapped directly onto the physical architecture, and the NN of the qubits is implemented using traditional quantum routing methods [30]. While this approach avoids the reliance on Hamiltonian paths, it requires more resources and time to implement the NN of quantum circuits, and may not lead to optimal solutions. In practical applications, these drawbacks may lead to lower efficiency in quantum computing or even failure to achieve the desired computational tasks.

With enhancing the fidelity as the goal, we propose a

solution for the NN synthesis of CNOT circuits on general quantum architectures. The main contributions of this paper are as follows.

- The challenges associated with CNOT quantum circuit synthesis on quantum architectures without Hamiltonian paths are analyzed, and a key-qubit priority mapping model is proposed to solve the problem. Based on this model, the initial mapping of key qubits is further improved by using tabu search to enhance the circuit fidelity after synthesis.
- Based on the initial mapping strategy of key qubits, an NN synthesis of CNOT circuits method is proposed for the general architecture. This method converges the Boolean matrix by layers under the premise of satisfying the NN constraint, and gradually realizes the matrix transformation, thus transforming into a CNOT circuit with a lower error rate.
- The above algorithm is implemented on several mainstream cloud quantum computing platforms, including real quantum computers and quantum simulators. The demonstration results show that, by employing noise-aware synthesis methods and reducing the number of CNOT gates, the fidelity of CNOT quantum circuits is significantly improved. Compared to current state-of-the-art synthesis methods, the fidelity is improved by 21.3% and 7.0% on IBMQ_QX5 and IBMQ_Tokyo, respectively. Compared to current mainstream cloud platform quantum compilers, the fidelity is improved by a factor of 5.7 and 243 on IBMQ_Qutio and IBMQ_Guadalupe, respectively. The fidelity of the Bernstein-Vazirani (BV) algorithm is improved by 14.8% on both the quantum computing devices and simulators.

This paper is organized as follows: in Section II, basic concepts involving CNOT circuit synthesis are briefly introduced. In Section III, key-qubit priority mapping for general quantum architectures is studied, a key-qubit priority model is established, and the key-qubit priority initial mapping is optimized by tabu search. In Section IV, a noise-aware CNOT circuit NN synthesis based on the key-qubit priority model is considered, and a CNOT circuit NN synthesis algorithm applicable to the general architecture is given. In Section V, the proposed method's optimization for circuit fidelity is verified by the execution results on quantum computing devices. The paper is discussed and summarized in Section VI and VII.

II. BACKGROUND

A. CNOT gate and CNOT circuit

The CNOT (Controlled-NOT) gate is a basic two-qubit quantum logic gate that performs a conditional NOT op-



FIG. 1. The CNOT gate and its unitary matrix.

eration on the target qubit depending on the state of the control qubit. Fig. 1 shows a graphical representation of a CNOT gate with two input qubits and its unitary matrix, where q_0 denotes the control bit and q_1 denotes the target bit. The operation of CNOT gate can be represented by a unitary matrix, which defines the relationship between input and output.

This unitary matrix shows that the CNOT gate flips the state of the target qubit if and only if the control qubit is in the $|1\rangle$ state, which can be expressed in Eq. (1).

$$|00\rangle \rightarrow |00\rangle; |01\rangle \rightarrow |01\rangle; |10\rangle \rightarrow |11\rangle; |11\rangle \rightarrow |10\rangle \quad (1)$$

Due to the capability of representing any multi-qubit gate by using a combination of CNOT gates and single-qubit gates, CNOT gates are frequently employed in quantum circuits for qubit state manipulation. A circuit consisting only of CNOT gates is called a CNOT circuit.

B. Quantum topology architecture

Although the number of qubits in NISQ devices has increased, they still face various physical constraints, including connectivity constraints and gate errors. The connectivity between different physical qubits can be represented by a quantum topology graph. Fig. 2 displays the coupling graph of two IBM NISQ device topologies. Coupling graphs for all the other architectures considered in the paper are shown in the Appendix A. Currently, the only two-qubit gate supported by IBM devices are CNOT gates, which can only operate on two qubits connected by an edge in the coupling graph. In other words, the logical qubits of the CNOT gate mapped onto these two connected physical qubits satisfy the NN constraint. Note that there is no Hamiltonian path in the two coupling graphs in Fig. 2.

Another physical constraint reflected in the coupling graph is the gate error. The weights on the edges of the topological graph indicate the error rates of gate operations between two qubits. Higher weights imply higher error rates. Additionally, due to the qubit quality parameter, the error rate between two adjacent qubits is also different, which leads to different error rates for CNOT gates acting on different qubits. Therefore, it is necessary to satisfy the connectivity constraint and to reduce the gate error when mapping quantum circuits.

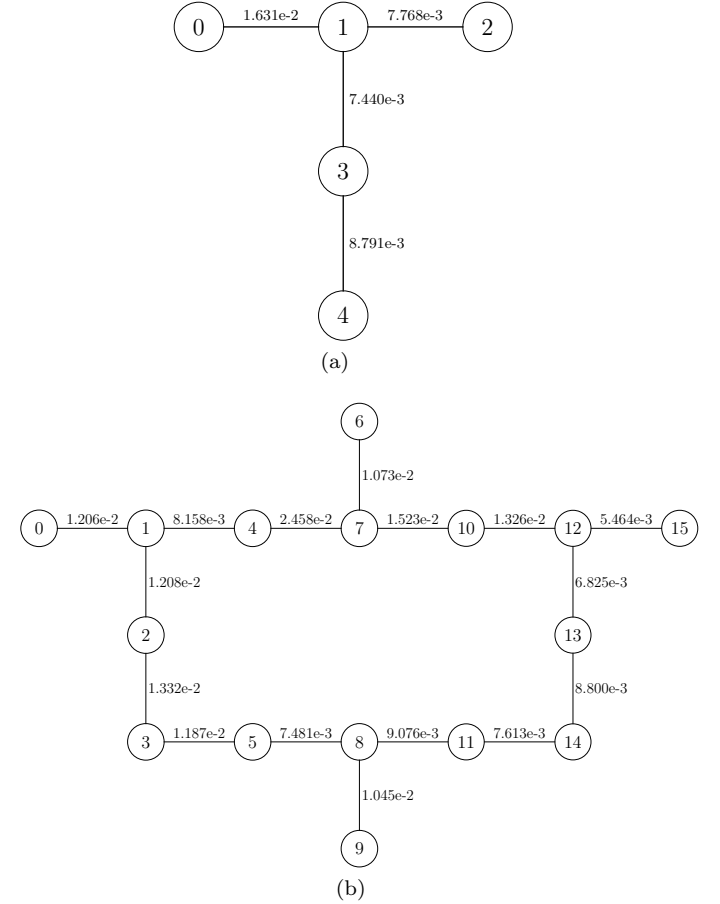


FIG. 2. Two coupling graphs of the IBMQ topology architecture, where each node represents a physical qubit and each edge represents that there is an interaction between the two qubits, and the values adhering to the edges are the error rates of the CNOT gates. (a) The IBMQ_Quito topology with 5 qubits. (b) The IBMQ_Guadalupe topology with 16 qubits.

C. Boolean matrix

The CNOT gate can be represented by a unitary matrix of size 4×4 . The matrix of a CNOT circuit containing n qubits requires a tensor product of the individual CNOT's unitary matrix, so a CNOT circuit with n qubits requires a matrix representation of size $2^n \times 2^n$. However, in the Boolean matrix representation of a CNOT circuit, the matrix size corresponds to the number of qubits. A CNOT circuit with n number of qubits corresponds to an $n \times n$ Boolean matrix. The Boolean matrix of the CNOT circuit is calculated as shown in Fig. 3.

The CNOT circuit shown in Fig. 4(a) consists of seven CNOT gates with five qubits, namely $\{q_0, q_1, q_2, q_3, q_4\}$. It can be represented as a 5×5 Boolean matrix, where $\{q_0, q_1, q_2, q_3, q_4\}$ correspond to $\{R_1, R_2, R_3, R_4, R_5\}$ and $\{C_1, C_2, C_3, C_4, C_5\}$ in the Boolean matrix, respectively. During the conversion process of Boolean matrix, several XOR operations are performed. Firstly, the control bit

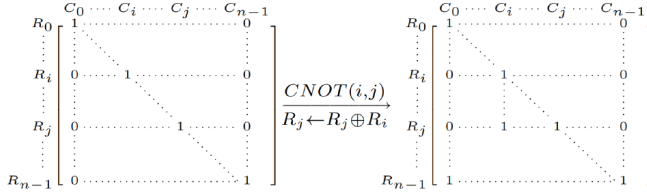
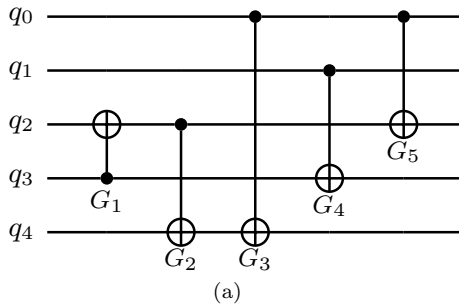
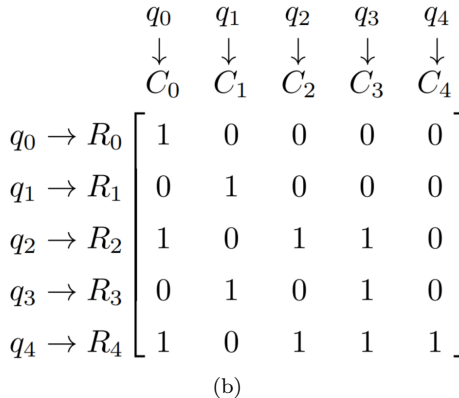


FIG. 3. To calculate the Boolean matrix of a CNOT circuit, the following steps can be followed. For any CNOT gate with n variables in the circuit, where the variable domain is $\{x_1, x_2, \dots, x_i, \dots, x_j, \dots, x_n\}$, with x_i as the control bit and x_j as the target bit. In an $n \times n$ identity matrix, the row i corresponding to the control bit x_i of each CNOT gate is XORed to the row j corresponding to the target bit x_j .



(a)



(b)

FIG. 4. A CNOT circuit and its Boolean matrix. (a) A CNOT circuit consisting of 7 CNOT gates. (b) Correspondence between the rows and columns of the Boolean matrix and the qubits.

q_3 of gate G_1 is XORed to the target bit q_2 and the result is stored in the target bit q_2 , which is expressed as $R_2 = R_2 \oplus R_3$ in the Boolean matrix. And then the control bit q_2 of gate G_2 is XORed to the target bit q_3 , which is expressed as $R_3 = R_3 \oplus R_2$ in the Boolean matrix. The same operation is carried out for G_2 to G_5 . The final Boolean matrix is shown in Fig. 4(b).

III. KEY-QUBIT PRIORITY INITIAL MAPPING STRATEGY

In order to extend the synthesis method with Hamiltonian path architectures, and solve the NN synthesis problem of CNOT circuits on the architecture without Hamiltonian paths, the nearest-neighbor synthesis of CNOT circuits on general quantum architectures is proposed to achieve the NN synthesis of CNOT circuits while ensuring the NN constraint. The NN synthesis of CNOT circuits on general quantum architectures is ultimately achieved through a noise-aware CNOT circuit NN synthesis strategy (Algorithm 4). This algorithm comprises two main components: initial mapping and matrix elimination. The initial mapping is conducted using a key-qubit priority initial mapping strategy (Algorithm 1) along with its optimized variant (Algorithm 2). Matrix elimination is implemented using a Steiner Tree approach and target-aided rows matching (Algorithm 3).

This section proposes a key-qubit priority mapping model that prioritizes and maps key qubits on a coupling graph. Additionally, tabu search is employed to optimize the initial mapping, aiming to reduce the number of CNOT gates and enhance the circuit fidelity.

A. Key-qubit priority model

An $n \times n$ Boolean matrix can be divided into n layers along its diagonals, where the first layer includes the first column and the first row, the i -th layer ($1 \leq i \leq n$) includes the i -th column and i -th row, up to the last layer which contains only one element. In the process of Boolean matrix elimination, a layer-first principle is followed, as shown in Fig. 5. The layer-first principle starts from the first layer and proceeds to the $(n-1)$ -th layer, and the elimination is carried out in the order of columns first and then rows. Ultimately, the Boolean matrix is transformed into an identity matrix, and the synthesized quantum circuit comprises a reverse cascade of all the CNOT gates applied throughout the transformation process.

Given that each layer of the Boolean matrix represents a qubit, processing the matrix layer by layer corresponds to the operation sequence $\{q_0, q_1, \dots, q_n\}$. The corresponding operation sequence in the initial mapping of the coupling graph is $\{q_0 \rightarrow Q_{i0}, q_1 \rightarrow Q_{i1}, \dots, q_n \rightarrow Q_{in}\}$. At every i -th step, it is necessary to remove vertex Q_i , ensuring that the diagonal elements of the matrix, post-layer operation, are not affected by subsequent synthesis processes. However, if the operation sequence in the coupling graph post-initial mapping does not form a Hamiltonian path, the step of removing vertices may result in the coupling graph being divided into two disconnected subgraphs. This division causes a loss of interaction paths between certain qubits, rendering the circuit unsynthesized. Therefore, it is crucial to find a reasonable initial mapping method that prevents the removal of ver-

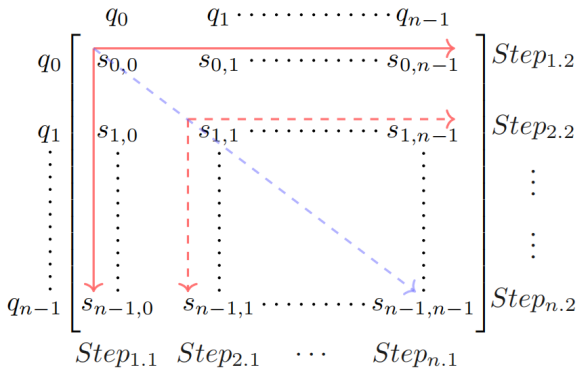


FIG. 5. Illustration of the Boolean matrix elimination process. The Boolean matrix is processed by layer and follows the principle of columns before rows.

tices from dividing the coupling graph into disconnected subgraphs.

Lemma 1. *Let $G = (V, E)$ be an undirected graph. If the removal of a vertex $v \in V$, along with all the edges associated with it, causes G to split into two or more disconnected subgraphs, then the vertex v is known as the cut point of graph G [31].*

In the coupling graph shown in Fig. 6, Q_1 and Q_3 are cut points. Their deletion from the coupling graph results in the splitting of the graph into multiple subgraphs, rendering the matrix elimination process infeasible. In order to perform matrix elimination operations accurately, it is necessary to map logical qubits with lower indexes to vertices that are not cut points in the physical quantum coupling graph in priority during the initial mapping. We refer to such vertices as key qubits.

Definition 1. *For a coupling graph $G = (Q, E)$ that contains several physical qubits, where $Q = \{Q_0, Q_1, \dots, Q_i, \dots, Q_{n-1}\}$ ($0 \leq i < n$), a vertex Q_i that is a non-cut point is regarded as the key physical qubit of the priority mapping, or the key qubit for brevity.*

To ensure the feasibility of matrix elimination, priority is given to the physical qubits that are non-cut points, known as key qubits, during the mapping process. For instance, in the IBMQ-Quito architecture, qubits Q_0 , Q_2 , and Q_4 are non-cutting points, which are the key qubits, as shown in Fig. 6. During the initial mapping, priority is given to map q_0 , q_1 , q_2 to these three physical qubits. If q_0 is the first qubit to be mapped to Q_0 , it becomes disconnected from the other qubits in the coupling graph after the first layer of matrix elimination is completed. By prioritizing the constraints of mapping key qubits, the key-qubit priority model can be satisfied while reducing the complexity of the initial mapping at the same time.

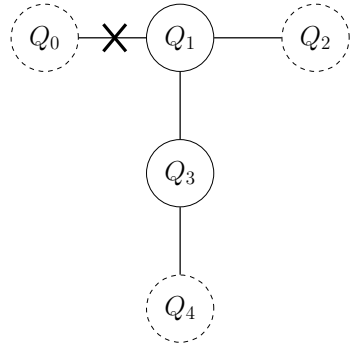


FIG. 6. An example of the key-qubit priority model for the IBMQ-Quito. The dashed qubits Q_0 , Q_2 , and Q_4 are non-cutting points, i.e., key qubits. These qubits need to be prioritized. Solid qubits Q_1 and Q_3 are cut points.

B. Key-qubit priority mapping based on tabu search

In order to avoid the occurrence of disconnected subgraphs in a coupling graph, this paper proposes a key-qubit priority mapping method. This method prioritizes the vertices that are not cut points, i.e., key points, on the coupling graph. Then the processed vertices and the edges connected to them are removed from the coupling graph until a complete Hamiltonian path exists in the updated coupling graph. After the deletion of a key qubit, a new subgraph is created. New key qubits may appear in this subgraph, which were not cut points in the original coupling graph. By considering the constraints of key qubits, a recursive algorithm for selecting and mapping the key qubits in the order of increasing logical qubits index can be provided in the analysis of the key-qubit priority model. This ensures that the logical qubits at the key qubits are prioritized in the subsequent elimination process. The key-qubit priority initial mapping algorithm KQPI is shown in Algorithm 1.

This algorithm takes the coupling graph G and the number of logical qubits n as input, and outputs a randomized key-qubit priority initial mapping. This algorithm takes the non-cut points in the coupling graph as key qubits and iterates through recursion, reducing the complexity of the initial mapping. However, it is worth noting that Algorithm 1 only outputs a single mapping scheme. With n qubits in a quantum computing architecture, there can be up to $n!$ possible initial mapping schemes, making it impractical to traverse each one by the brute force search method. Although the key-qubit priority initial mapping algorithm can reduce the search space of initial mappings, it may still not be able to find the optimal initial mapping quickly considering the increasing size of physical qubits on quantum computing devices. In this case, a better balance between solution accuracy and speed can be achieved with the help of metaheuristic algorithms.

This work utilizes a tabu search algorithm to solve

Algorithm 1: Key-qubit priority initial mapping (KQPIIM)

Input: The coupling graph $G = (V, E)$, the initial map π , the number of logical qubits n , the list of initial key qubits $ikey_list$

Output: The initial map π_0

```

1 begin
2   |  $i \leftarrow \text{Nodes}(G_0) - \text{Nodes}(G)$ ;
3   | if  $G \exists \text{ Hamilton path}$  then
4   |   | foreach  $Q_i$  in  $\text{Hamilton path}$  do
5   |   |   | add  $\{i : Q_i\}$  to  $\pi$ ;
6   |   |   |  $i++$ ;
7   |   | end
8   |   | return  $\pi$ ;
9 end
10 if  $\pi = \text{null}$  then
11   |   |  $key\_list \leftarrow ikey\_list[0]$  ;
12   |   |  $G \leftarrow G / ikey\_list[0]$ ; /* Delete point from  $G$ 
13   |   | */
14 end
15 foreach  $Q$  in  $V$  do
16   |   |  $key\_list \leftarrow Q$  is non-cut points;
17 end
18 if  $G \not\exists \text{ Hamilton path}$  then
19   |   |  $key\_qubit \leftarrow key\_list[\text{random}]$ ;
20   |   | add  $\{i : key\_qubit\}$  to  $\pi$ ;
21   |   |  $G \leftarrow G / key\_qubit$ ;
22   |   |  $i++$ ;
23 end
24 if  $\text{len}(\pi) != n$  then
25   |   | KQPIIM( $G, \pi, n, ikey\_list$ );
26 end

```

the initial mapping problem for CNOT circuit synthesis. Tabu search guides the search toward a more optimal region of the search space by maintaining a tabu table, while avoiding exploring suboptimal solutions previously [32]. The algorithm iterates and updates the tabu table as it explores the solution space, gradually improving the quality of the found solution until a satisfactory solution is found or the maximum number of iterations is reached. Since the elimination of the Boolean matrix under topological constraints requires considering not only the CNOT cost under the NN constraint but also the overall fidelity of the circuit. The number of CNOT gates is highly correlated with the connectivity of the qubits in the coupling graph. Low qubits connectivity can necessitate more CNOT gates to complete the NN. On the other hand, the error rate of CNOT gates is a crucial factor affecting the fidelity of the circuit. Choosing qubits with a lower error rate for mapping is beneficial for building circuits with high fidelity. The objective function F_π of the optimization method is defined in Eq. (2),

$$F_\pi = \prod_{0 \leq i < j < n} \frac{\sum_{v \neq i, j} \frac{C_v(i, j)}{C_v}}{C_{ij}} - \sum_{m=0}^{n-1} (m+1) \frac{\sum_{w \in E(\pi_m)} w}{|E(\pi_m)|} \quad (2)$$

where n denotes the number of qubits, $C_v(i, j)$ denotes the number of shortest paths through vertex v that contain both vertices i and j , C_v denotes the number of shortest paths through vertex v , C_{ij} denotes the number of shortest paths through i and j . m denotes the index number in the mapping method π , π_m denotes the m -th physical qubit in the mapping method π , $E(\pi_m)$ denotes the edge connected to the qubit π_m in the coupling graph, and w denotes the weight on this edge, i.e., the error rate.

The first half of Eq. (2) represents the degree of connectivity of the mapped qubits in terms of connectivity factors. This part is used to measure the connectivity of the sub-coupling graph when the physical qubits are not fully mapped. The inter-vertex connectivity factor is one of the indicators of the connectivity between vertices in a graph. The connectivity factor can be calculated by using the Betweenness Centrality algorithm in graph theory [33]. It ranges from 0 to 1, where 0 indicates that two vertices are not connected. A higher connectivity factor indicates stronger connectivity and fewer CNOT gates required to act on the two qubits. And the second half of Eq. (2) represents the fidelity profile of the mapped qubits. According to the key-qubit priority model, the more advanced qubits in π are removed first, and the error rate associated with these qubits also have less impact on the circuit. To distinguish the importance of the error rates between different qubits, $m+1$ is assigned as the weight of these error rates. The later the qubits in π are removed, i.e., the larger m is, the greater the number of CNOT gates acting on these qubits, hence, the greater the impact on circuit fidelity. Therefore, the weights of these qubits are set through $m+1$.

The objective function Eq. (2) directly addresses the dual objectives of optimizing qubit connectivity and minimizing error rates to enhance the overall fidelity of the quantum circuit. High connectivity among qubits typically suggests fewer CNOT gates are required, potentially reducing the circuit's overall execution time and complexity. However, high connectivity does not automatically guarantee high fidelity; the error rates associated with the qubits and their connections play a critical role. High error rates can significantly degrade the circuit's fidelity, negating the benefits of high connectivity. Therefore, the objective function Eq. (2) is designed to balance these considerations by weighing both the connectivity of qubits and their fidelity profiles. This balanced approach allows for the identification of qubit mappings that not only ensure efficient quantum gate implementations but also maintain high circuit fidelity. By simultaneously optimizing for connectivity and error rates, Eq. (2) serves as a comprehensive cost function that guides the tabu search algorithm towards finding mappings that achieve high-fidelity quantum circuit designs under practical constraints.

After the cost function has been determined, the initial mapping of CNOT circuit synthesis is optimized by tabu search algorithm. Firstly, a tabu table of length

N is initialized, and the mapping method π_0 of Algorithm 1 (KQPIM) is added to the tabu table. Secondly, a set of candidate solutions is generated, namely multiple mapping methods $\pi_\Delta = \{\pi_1, \pi_2, \dots, \pi_n\}$, by randomly disturbing the initial key qubits in π_0 . These initial key qubits are the non-cut points of the uncut coupling graph, and these qubits form the `ikey_list`. Disturbing only the `ikey_list` ensures that the key qubit priority model is satisfied. Next, the mapping schemes in π_Δ that already exist in the tabu table are removed, and the mapping schemes whose cost F_π is lower than the average cost in the tabu table are added to the tabu table. Finally, the tabu table is updated to remove the mappings with higher cost F_π in the tabu table. This cycle continues until the end of the iteration. The pseudo-code for the tabu search algorithm to optimize the initial mapping of CNOT circuit synthesis is provided in Algorithm 2.

Algorithm 2: Key-qubit priority initial mapping optimization (KQPIMO)

Input: The coupling graph $G = (V, E)$, the number of logical qubits n
Output: The best initial map π_{best}

```

1 begin
2    $T\_list \leftarrow [] * N$ ,  $\pi \leftarrow []$ ;
3   ikey_list  $\leftarrow$  non-cut points in  $G$ ;
4    $\pi_0 \leftarrow KQPIM(G, \pi, n, ikey\_list)$ ;
5   add  $\pi_0$  to  $T\_list$ ;
6   for  $i < iterations$  do
7      $\pi_\Delta \leftarrow []$ ;
8     for  $k = 0$  to  $N$  do
9       // Change only key qubits
10      ikey_list  $\leftarrow$  random disturbance key qubits
11        in ikey_list;
12       $\pi_k \leftarrow KQPIM(G, \pi, n, ikey\_list)$ ;
13      add  $\pi_k$  to  $\pi_\Delta$ ;
14    end
15    foreach  $\pi$  in  $\pi_\Delta$  do
16      if  $\pi \notin T\_list$  and  $F_\pi \leq F_{avg(T\_list)}$  then
17        | add  $\pi$  to  $T\_list$ ;
18      end
19      if size( $T\_list$ )  $> N$  then
20        |  $T\_list \leftarrow$  update( $T\_list$ )
21      end
22    end
23     $\pi_{best} \leftarrow$  best( $T\_list$ );
24  return  $\pi_{best}$ ;
25 end

```

The key-qubit priority initial mapping optimization algorithm based on tabu search described above is an iterative optimization method. It helps to improve the optimization rate and fidelity of quantum circuits by setting a reasonable length of the tabu table and the number of iterations. This enables the mapping method to trade off a certain amount of time cost for the enhancement of the overall quality of the circuit.

IV. KEY QUBIT-AWARE CNOT CIRCUIT NN SYNTHESIS

This section presents an NN synthesis method based on the key-qubit priority initial mapping strategy. The method improves the synthesis efficiency by prioritizing the mapping and elimination processing of key qubits. It enables the implementation of CNOT circuit NN synthesis on an architecture with and without Hamiltonian paths. And at the same time, the fidelity of the NN synthesized circuits is improved as much as possible. Specifically, the target-aided rows matching algorithm is introduced firstly, which helps to find the best auxiliary row to achieve row elimination of Boolean matrix. Next, this section describes the noise-aware CNOT circuit NN synthesis algorithm based on layer convergence, which uses a layer-by-layer elimination method. Finally, an algorithm example is provided to facilitate a better understanding of the application and effect of the algorithm.

A. Target-aided rows matching algorithm

In the key-qubit priority mapping model, the processed vertices need to be removed from the coupling graph. Consequently, the elimination must process not only the current column but also the current row. In order to change the values of the elements in the current row other than those on the main diagonal to 0, it is necessary to use the auxiliary of other rows in the matrix to perform an XOR operation with the current row. The set of target-aided rows found based on the current row is presented in Definition 2..

Definition 2. Consider an invertible Boolean matrix. Let R_i be the current row and e_i be its corresponding unit row vector, defined such that $e_{ij} = 1$ if $j = i$ and $e_{ij} = 0$ otherwise. Define the set Set_k comprising rows R_k for which the $\bigoplus R_k = R_i \oplus e_i$ holds, where $i < k \leq n$ and n is the number of rows in the matrix. This set is referred to as the target-aided rows set.

Example 1. Fig. 7 illustrates an example of matching the target-aided rows. At this point, the rows of the first layer and the columns of the second layer of this matrix have been processed, and the next step is to complete the row elimination of the second layer. According to Definition 2, it is necessary to match to the set of target-aided rows that satisfy the condition $\bigoplus R_j = R_1 \oplus e_1$, where $e_1 = [0, 1, 0, 0, 0]$. After calculating, the target-aided rows set of R_1 is $\{R_3, R_4\}$.

In the case where the matrix is invertible, the system of linear equations $Ax = y$ must have a unique solution. Therefore, if the target row exists, the set of target-aided rows must be found, i.e., the target-aided rows matching is completed. Specifically, the set of target rows can be determined by solving the system of linear equations. If the system of linear equations has a solution, it means

q_0	q_1	q_2	q_3	q_4	
q_0	1	0	0	0	0
q_1	0	1	1	0	1
q_2	0	0	0	1	0
q_3	0	0	1	0	0
q_4	0	0	0	0	1

FIG. 7. Target-aided rows matching example. By calculating $R_1 \oplus e_1 = [0, 0, 1, 0, 1]$, the set of target-aided rows must be matched to obtain $\bigoplus R_j = [0, 0, 1, 0, 1]$. And the set $\{R_3, R_4\}$ satisfies $R_3 \oplus R_4 = [0, 0, 1, 0, 1]$, therefore, the target-aided rows set of R_1 is $\{R_3, R_4\}$.

that the target rows set exists, and we only need to find the rows corresponding to the non-zero elements in the solution vector. Based on the above analysis, a target-aided rows matching algorithm is given, as shown in Algorithm 3.

Algorithm 3: Target-aided rows matching (TARM)

Input: The invertible boolean matrix M , the target row index i
Output: The target auxiliary row index list R_j

```

1 begin
2   // Get the rank of the matrix
3   n ← r(M);
4   // Initialize list to generate permutations
5   L ← [], R_list ← [];
6   for m = i to n do
7     // Generate the index sequence to be
     // matched according to the target row
     // index
8     add m to L;
9   end
10  for length = i to n do
11    // save current permutation
12    R_list ← Prem.append(L, length);
13  end
14  foreach  $R_j$  in R_list do
15    if  $\bigoplus R_j = R_i \oplus e_i$  then
16      | return  $R_j$ ;
17    end
18  end
19 end

```

To construct the set of target-aided rows, the algorithm first generates the sequence of indexes to be matched in accordance with the target row index. Next, the algorithm searches for feasible solutions through the full permutations of all rows, except for the target row. The full permutation of l numbers from the set L can be expressed as $\text{Perm}(L, l)$. So the complexity of lines 7-8 in

Algorithm 3 is shown in Eq. (3).

$$O\left(\sum_{l=0}^n \frac{n!}{(n-l)!}\right) = O\left(n! \sum_{l=0}^n \frac{1}{l!}\right) \quad (3)$$

where n denotes the number of qubits. The value of $\sum_{l=0}^n \frac{1}{l!}$ in Eq. (3) must be less than 3, and it is a constant. In addition, the complexity of the summation operation in line 11 of Algorithm 3 is $O(n)$, and this operation is nested within $O(n!)$. Therefore, the complexity of Algorithm 3 is $O(n \cdot n!)$.

B. Noise-aware CNOT circuits NN synthesis strategy

The synthesis of CNOT circuits can be accomplished by using the Steiner tree model and Gaussian elimination to convert the Boolean matrix M of the CNOT circuit to an identity matrix I . Within the quantum coupling graph, each column of the Boolean matrix with qubits represented by the value 1 can be used to construct a Steiner tree. This Steiner tree includes all qubits (terminal nodes) with a value of 1 as well as auxiliary qubits (Steiner nodes). The construction of the Steiner tree has been proven to be an NP-complete problem [34]. Subsequent row operations in Gaussian elimination are constrained by the edges of the Steiner tree, thus ensuring that the corresponding CNOT gates adhere to the connectivity constraints of the architecture.

Definition 3. In Gaussian elimination, a CNOT gate modifies matrix elements. To switch element S_i from 0 to 1 using $S_j = 1$, apply $S_i \leftarrow S_i \oplus S_j$ by a CNOT gate $\text{CNOT}(S_j, S_i)$, denoted as $\text{set1}[S_i, S_j]$, achieving $0 \oplus 1 = 1$. Similarly, to set S_i from 1 to 0, use $S_i \leftarrow S_i \oplus S_j$, noted as $\text{set0}[S_i, S_j]$, resulting in $1 \oplus 1 = 0$.

Based on the preceding elimination rules, the Boolean matrix M must be processed sequentially by column. A Steiner tree is constructed for each i -th column of the matrix. The set1 or set0 operation is then employed to convert all non-zero elements in each column to 0, except for the i -th element, which is transformed to 1.

Example 2. Taking the circuit in Fig. 4(a) as an example, the circuit is mapped onto the coupling graph in Fig. 2(a) in the default initial mapping $\{q_0 \rightarrow Q_0, q_1 \rightarrow Q_1, q_2 \rightarrow Q_2, q_3 \rightarrow Q_3, q_4 \rightarrow Q_4\}$. The first column of the Boolean matrix M , which represents this circuit, is processed first. A Steiner tree is constructed for the elements of the first column. In this Steiner tree, q_0 acts as the root node, and q_2 and q_4 are the leaf nodes. The Steiner tree is then post order traversed, and the sequence of qubits elimination is q_4, q_2, q_0 . While eliminating q_4 , it is not possible to convert q_4 to 0 by using $\text{set0}(q_4, q_3)$ because the state of q_3 , which is adjacent to q_4 , is 0. Therefore, $\text{set1}(q_3, q_4)$ is used to convert q_3 to 1, followed by the execution of $\text{set0}(q_4, q_3)$. The corresponding CNOT operations are $\text{CNOT}(4,3)$ and $\text{CNOT}(3,4)$. Similarly, the

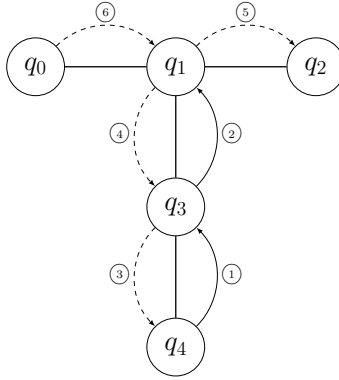


FIG. 8. The NN synthesis process in the IBMQ_Quito architecture for the circuit of Fig. 4(a). The numbering indicates the order of the sets, the dotted arrows indicate *set0*, the solid arrows indicate *set1*.

same operation is performed on the other qubits until only q_0 is 1 in the first column of this matrix. The process of synthesis of the first column is shown in Fig. 8. The numbers indicate the order of the set operations, the solid arrows indicate *set1*, the dashed arrows indicate *set0*.

Given that quantum algorithms involve many two-qubit operations, the error of each two-qubit operation, i.e., the two-qubit gate, is more significant compared to single-qubit operations. In order to maximize the probability of successful execution of the synthesized CNOT circuits on real quantum computing devices, the error of each inserted CNOT gate must be considered during the synthesis of CNOT circuits. A noise-aware CNOT circuit NN synthesis method is proposed to mitigate these unavoidable noise problems.

In the process of matrix elimination, multiple interaction paths may occur when Gaussian elimination is performed between two qubits that are not close neighbors. Since the error rates between neighboring qubits on different paths are different, choosing different interaction paths to build Steiner trees can cause different errors in the results. To measure the error cost of each interaction path, we propose an interaction path fidelity measure F_{path} , as shown in Eq. (4).

$$F_{path} = \prod_{Q_i, Q_j \in path} (1 - E[Q_i][Q_j]) \quad (4)$$

where Q_i and Q_j are the two qubits that are near neighbors on the interaction path, and $E[Q_i][Q_j]$ denotes the two-qubit gate operation error rate, i.e., the weight of the edge on the coupling graph. A larger F_{path} indicates a higher fidelity on this interaction path, which means that the integrated CNOT quantum circuit can obtain a better reliability.

In order to verify the accuracy of the fidelity calculation method in Eq. (4), the fidelity calculated from the simulations is compared with the fidelity of the actual

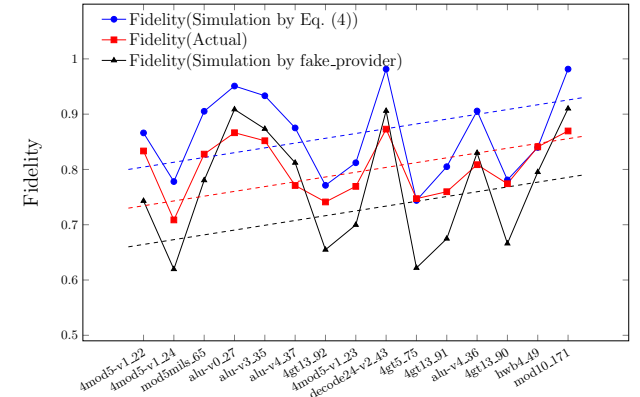


FIG. 9. Actual fidelity versus simulated fidelity on IBMQ_Quito. The red curve represents the fidelity achieved through execution on an actual quantum computing device IBMQ_Quito, the black curve represents the fidelity of IBMQ_Quito simulation using qiskit's `fake_provider` simulator, and the blue curve corresponds to the fidelity simulated using Eq. (4).

quantum hardware after implementation, and the results are shown in Fig. 9. By comparing the fidelity of 15 circuits from RevLib [35], whose circuit sizes range from 11 to 108, it is found that the simulated fidelity shows essentially the same fluctuations and trends as the actual fidelity, but the simulated fidelity is slightly higher than the actual fidelity. This phenomenon can be attributed to the existence of some specific noise and errors in the actual quantum hardware, such as crosstalk, measurement errors, and some other quality parameters of the qubits that may change over time. These factors worsen the error rate and lower the actual fidelity of the synthesized CNOT circuits. Similarly, the fidelity of simulated circuits executed in the Qutio architecture using `fake_provider` in qiskit shows the same fluctuations and trends. Demonstration results on the IBMQ_Quito computing device show that the F_{path} can predict the execution fidelity of the quantum circuit effectively.

After considering the hardware noise, the interaction path selection problem can be transformed into a search for the path with the highest metric F_{path} among all paths between two qubits. This problem can be solved by the Dijkstras algorithm. The two qubits of the *set0* or *set1* action are used as the start and finish qubits in the interaction path selection strategy based on the Dijkstras algorithm. The strategy visits adjacent qubits from the start qubit and calculates F_{path} , then looks for higher F_{path} vertices until the end qubit is visited. When there is only one interaction path between the start qubit and the end qubit, this path is the one with the highest F_{path} . This path selection strategy provides an interaction path with the highest fidelity for two logical qubits that are not adjacent to each other, so that the set operation acting on this interaction path has the lowest error rate and reduces the effect of errors in the matrix elimination process.

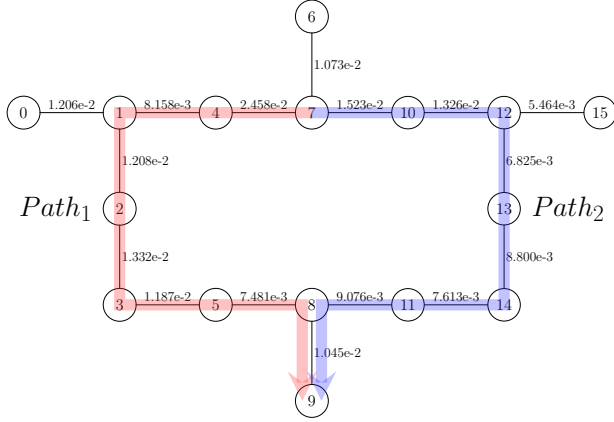


FIG. 10. There are two interaction paths between Q_7 and Q_9 in the IBMQ_Guadalupe. The simulated fidelity of the two interacting paths is calculated by Eq. (4), and it is found that the fidelity of F_{path_2} is higher, so the fidelity of the CNOT gates acting on F_{path_2} is higher than those CNOT gates on F_{path_1} . At this point, F_{path_2} is the better elimination path.

Example 3. Suppose a circuit is mapped to the coupling graph in Fig. 2(b), and the two qubits mapped to Q_7 and Q_9 need to be eliminated, where the qubit mapped to Q_7 is the main diagonal element and the qubit mapped to Q_9 is 1 in the matrix. So Q_7 is the root node of the Steiner tree, and Q_9 is the child node. Since Q_7 and Q_9 are not adjacent, the *set0* operation cannot be directly performed. Therefore, it is necessary to gradually apply *set1* to all qubits on the path from Q_7 to Q_9 . At this point, there are two interactive paths available, $path_1$ is (7-4-1-2-3-5-8-9), and $path_2$ is (7-10-12-13-14-11-8-9). The two interaction paths are shown in Fig. 10. To determine the optimal path, we calculate F_{path_1} and F_{path_2} respectively, and find that F_{path_2} is greater than F_{path_1} . Therefore, $path_2$ is selected as the interactive path.

A minimum spanning tree for elimination is built by using the Steiner tree method, with the primary diagonal element serving as the root node. Vertices with a value of 1 in the current row or column are processed in turn, and the least weighted interaction path between these vertices and the tree is identified. All vertices on the path are then added to the tree until it contains all vertices with a value of 1. The minimum spanning tree obtained based on the above-mentioned method is referred to as a minimum-noise Steiner tree (MNST). Once minimum noise Steiner trees have been constructed for each row or column of the matrix, the matrix can be eliminated. The key-qubit priority initial mapping algorithm ensures the connectivity between the qubits during the matrix transformation. The target row matching algorithm solves the problem of finding the set of auxiliary rows of the elimination elements when processing row elimination elements. The specific flow of the NN synthesis algorithm for CNOT circuits on the general architecture is shown in Algorithm 4.

The algorithm processes the row and column of the

Algorithm 4: Nearest Neighbor Synthesis Algorithm for CNOT Quantum Circuits Based on Layer Convergence (LCNNS)

Input: The boolean matrix M , the qubit coupling diagram $G = (V, E)(|V| = n)$
Output: The CNOT gate sequence applied in row operation

```

1 begin
2   CNOT_list ← [];
3   π ← KQPIMO(G, n);
4   V_list ← π;
5   foreach i in V_list do
6     // Minimum noise Steiner tree
8     implemented by Dijkstra
9     T ← MNST(G, j|Mji = 1);
10    col_post_list ← postorder traverse T from i;
11    // Set the points in T with a value of 0
12    to 1
13    foreach c in col_post_list do
14      k ← c.parent;
15      if Mki = 0 and Mci = 1 then
16        Mk ← Mk ⊕ Mc;
17        CNOT_list.append([c, k]);
18      end
19    end
20    // Set points in T other than the root
21    node to 0
22    foreach c in col_post_list do
23      l ← c.children;
24      Ml ← Ml ⊕ Mc;
25      CNOT_list.append([c, l]);
26    end
27    Sj ← TARM(M, i);
28    T' ← Sj ∪ i;
29    row_pre_list ← preorder traverse T from i;
30    // Set the points in T' with a value of
31    0 to 1
32    foreach r in row_pre_list do
33      if r ∉ Sj then
34        k ← r.parent;
35        Mk ← Mk ⊕ Mr;
36        CNOT_list.append([r, k]);
37      end
38    end
39    row_post_list ← postorder traverse T from i;
40    // Set points in T' other than the root
41    node to 0
42    foreach r in row_post_list do
43      k ← r.parent;
44      Mk ← Mk ⊕ Mr;
45      CNOT_list.append([r, k]);
46    end
47    // remove qubit i from G
48    G ← G/i;
49  end
50  return CNOT_list;
51 end

```

current main diagonal element according to the layer convergence direction. First, the algorithm generates the initial mapping method π by algorithm 3 (line 3). When processing column elements, the algorithm generates a minimum noise Steiner tree based on the elements with a value of 1 in the current column (line 6). If a Steiner point exists, the child node is used to set the Steiner point to 1 (lines 8-14), and then the algorithm performs a post-order traversal to remove the main diagonal elements by *Set0* (lines 15-19). When processing row elements, the algorithm employs the target auxiliary row matching algorithm to find the row set used to assist elimination (line 20). Then a Steiner tree is generated based on the current row and the auxiliary row set (line 21). If a Steiner point exists, the algorithm uses the child node to set the Steiner point to 1 by *Set1* (lines 23-29). And finally, the algorithm sets the elements of the current row except the main diagonal to 0 by traversing the Steiner tree in post order (lines 31-35). After processing the row and column corresponding to the current qubit, the algorithm removes the current qubit and the edges connected to it from the coupling graph (line 36). Throughout the elimination process, the CNOT gate corresponding to each row and column operation is recorded.

The following is the complexity analysis, let n be the number of qubits in the coupling graph. The Steiner tree is generated by the Dijkstra algorithm (line 5), and the time complexity is $O(n^2)$. The time complexity of traversing the Steiner tree (line 6) is $O(n^2)$. The operations in the first foreach loop (lines 7-11) have constant time complexity, so the time complexity of the foreach loop is $Q(n)$. Similarly, the time complexity of the foreach loop (line 14) is also $Q(n)$. The time complexity of the TARM algorithm (line 19) is $Q(n \cdot n!)$. A new tree is constructed by using the Prim algorithm (line 20), and the time complexity is $O(n^2)$. The time complexity of obtaining the preorder traversal list (line 21) is $Q(n)$. The time complexity of the two foreach loops (lines 22 and 30) are both $Q(n)$. The time complexity of traversing the list (line 28) is $O(n^2)$. So the total time complexity of algorithm 4 is shown in Eq. (5).

$$\begin{aligned} & O(n(n^2 + n^2 + n + n!n + n^2 + n + n^2 + n)) \\ & = O(4n^3 + n^2n! + 4n) \end{aligned} \quad (5)$$

where n represents the number of qubits in the coupling graph. In summary, the time complexity of Algorithm 4 is dominated by the time complexity of the TARM algorithm. The complexity is further simplified to $O(n^2n!)$.

C. Algorithm example

To illustrate the NN synthesis process, we consider the CNOT circuit shown in Fig. 4(a) and use the IBMQ_Quito architecture as an example. The synthesis process is presented in Fig. 11. According to the key-qubit priority initial mapping optimization algorithm,

the initial mapping $\{q_0 \rightarrow Q_0, q_1 \rightarrow Q_4, q_2 \rightarrow Q_3, q_3 \rightarrow Q_1, q_4 \rightarrow Q_2\}$ that satisfies the key-qubit priority model is obtained.

First, the algorithm processes the first row of the first column. The first column of the 1 element corresponds to the qubits q_0, q_2, q_4 . The Steiner tree is generated in the coupling graph, and the algorithm performs post-order traversal of the current Steiner tree. If the current node value is 1 and the parent node value is 0, the current node is used to set its parent node to 1. So q_4 is used to set q_3 to 1 first, and CNOT(4,3) is executed. Next, the entire Steiner tree is traversed posteriorly, and q_4, q_2 , and q_3 are traversed in order to apply the parent node of the current node to the current row, i.e., CNOT(3,4), CNOT(3,2), and CNOT(0,3) are applied. Because the first row is already a unit vector, there is no need to process the first row.

Next, the second column and the second row are processed. The qubits corresponding to the 1 element in the second column are q_1, q_2, q_3, q_4 . The Steiner tree is generated in the coupling graph, and the current Steiner tree is traversed in the post-order. There are no Steiner points in the current Steiner tree, so no operation is needed. Then, the algorithm post-order traverses the whole Steiner tree, traverses q_4, q_3, q_2 in turn, and applies the row where the parent node of the current node is located to the current row, i.e., applies CNOT(3,4), CNOT(3,2), CNOT(1,2). Since the second row is already a unit vector, there is no need to process the second row.

Finally, the third column and the third row are processed. The qubits corresponding to the 1 element in the third column are q_3 and q_4 . The Steiner tree is generated in the coupling graph, and the current Steiner tree is traversed in the post-order. The qubit q_3 is used to set q_2 to 1 first, and then apply CNOT(3,2). Then, the algorithm traverses the whole Steiner tree in post-order, traverses q_4 and q_3 in turn, and applies the row where the parent node of the current node is located to the current row, that is, applies CNOT(3,4), CNOT(3,2). At this point, the third row is not a unit vector and needs to be processed. By using the target-aided rows matching algorithm, the third row can be obtained from the fifth row and the unit matrix $e_i = [0, 0, 1, 0, 0]$. So the Steiner tree is generated based on q_2, q_4 . After the first preorder traversal of the Steiner tree, because q_3 is not in the set of target rows, it is necessary to apply the corresponding row of q_3 to the corresponding row of q_4 , i.e., apply CNOT(3,4). Then the algorithm post-order traverses the Steiner tree, traverses q_4 and q_3 in turn, and applies the row where the current node is located to the row where the parent node is located, i.e., apply CNOT(4,3), CNOT(3,2). At this point, the whole matrix becomes a unit matrix, and the NN synthesis ends.

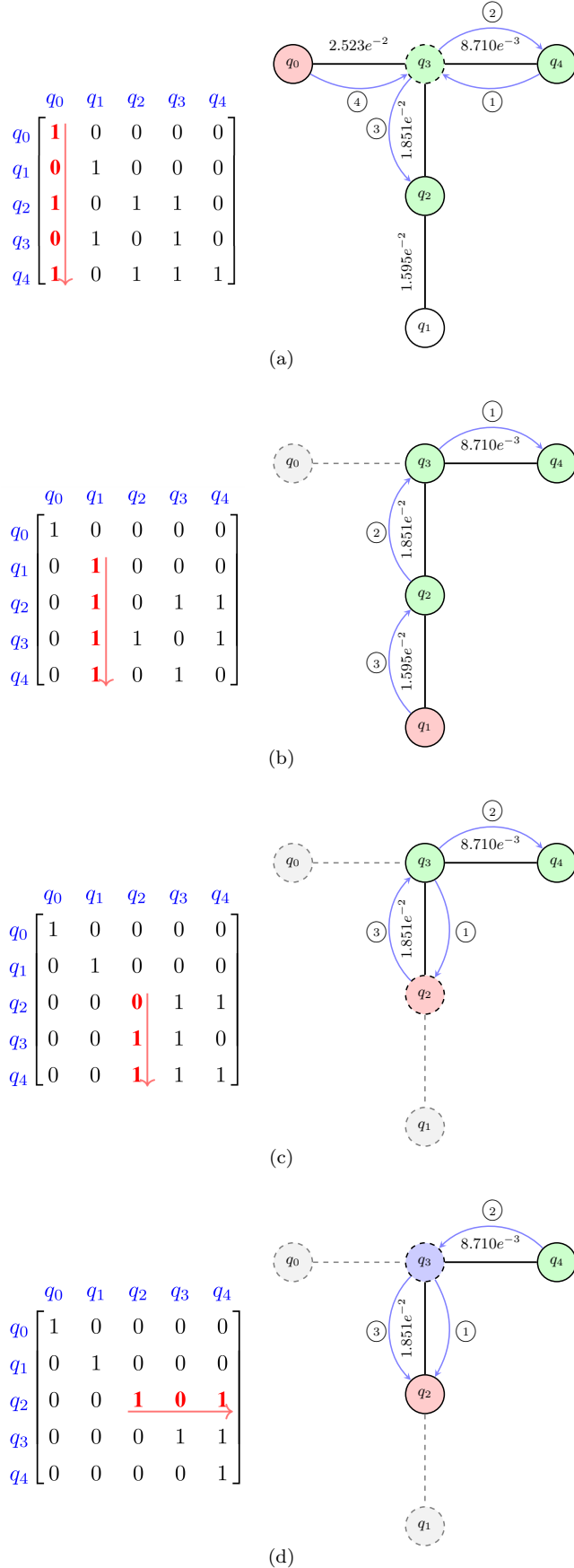


FIG. 11. Example of synthesis process for the circuit in Fig. 4(a).

V. DEMONSTRATION RESULTS AND ANALYSIS

In this section, the performance of the proposed synthesis method is evaluated using various metrics. The configurations used for the evaluations are first provided, followed by a detailed presentation of results for synthesis algorithm across various benchmarks. A specific analysis of these results is then conducted to highlight the effectiveness of the synthesis method.

A. Demonstration configurations

- 1) Runtime Environment: The algorithms are all implemented in Python language, and the code environment is the macOS Big Sur (11.2.3) operating system with Apple M1 Pro octa-core processing and 16GB RAM.
- 2) Quantum Computing Resources: The quantum cloud platforms used for the demonstration include OriginQ [36], Quafu [37] and IBMQ [38]. The coupling graphs and detailed parameters of the quantum computing devices on these platforms are shown in Appendices A and B.
- 3) Benchmarks: First, the 16- and 20-qubit random CNOT circuits given in [23] are demonstrated on the QX5 and Tokyo fake-provider simulators, respectively, with CNOT gate sizes of 4, 8, 16, 32, 64, 128 and 256. Secondly, a selection of randomly generated CNOT circuits including 5 and 16 qubits, with gate levels ranging from 10 to 10,000, is chosen for demonstrated on the Quito and Guadalupe fake-provider simulators, respectively. Finally, the synthesis of the Bernstein-Vazirani algorithm on different platforms with different architectures is utilized to illustrate the generality of the proposed method.
- 4) Metrics: CONT, the number of CNOT gates following synthesis; Depth, the depth of the circuit following synthesis; and Fidelity, the circuit fidelity following synthesis. For a circuit consisting of pure CNOT gates, the calculation of fidelity is defined as the ratio of the number of simulations where the output states remain all zeros to the total number of simulations. This fidelity is calculated by Eq. (6),

$$F = \frac{N_{\text{zero}}}{N_{\text{total}}} \quad (6)$$

where N_{zero} represents the number of simulations in which the output states remain all zeros, and N_{total} represents the total number of simulations. This approach is suitable for studies using CNOT circuits, as the ideal output for all-zero input states is also all zeros, making this ratio an effective measure of the circuit's fidelity under noisy conditions.

It is important to note that this definition of fidelity is specifically the ratio of successful all-zero output states to the total number of simulations, and should not be confused with other variants like estimated success probability (ESP) or total variance distance (TVD). For circuits containing single-qubit gates, ESP or TVD are better ways to calculate fidelity.

B. Demonstration results

1. Comparison with synthesis

In this part, the performance of the proposed LCNNS method is evaluated by comparing it with the synthesis approaches presented in Refs. [23], [26], and [28]. The comparison is carried out on the QX5 and Tokyo fake_provider simulators, respectively. The CNOT circuits, as introduced in the first part of the benchmarks, are utilized for this evaluation. For each circuit size, 20 instances are considered, and the results are averaged across these instances. In addition, circuit fidelity is performed by the fake_provider simulator [39], which is part of the Qiskit development package provided by the IBMQ cloud platform. The fake_provider simulator contains important information about the quantum system, such as coupling map, basis gates, qubit properties (T1, T2, error rate, etc.) which are essential for performing noisy simulation of the system.

The results, shown in Fig. 12, indicate that on the QX5 architecture, as the number of initial CNOT gates increases, the number of synthesized CNOT gates is lower than that of the comparison methods, and the fidelity is also higher. This trend becomes more evident as the number of CNOT gates increases. Specifically, on the QX5 architecture, the LCNNS method achieves a 21.3% improvement in fidelity over the other methods. On the Tokyo architecture, the methods proposed in [23] and [26] are more suitable for architectures that include Hamiltonian paths. In contrast, the methods in [28] and the LCNNS sacrifice the advantage in gate count for the generality of the architecture. Therefore, the synthesized CNOT gate count in [28] and the LCNNS method is higher than that of other comparison methods. Despite this increased gate count, the noise-aware LCNNS method maintains superior fidelity, achieving an average improvement of 7.0% over the best competing methods. The overall average optimization rate across both the QX5 and Tokyo architectures is 14.2%. This result demonstrates that the LCNNS method can effectively optimize circuits on both architectures, particularly showing advantages in maintaining quantum state fidelity.

2. Comparison with compilers

The second part of the benchmarks is implemented on the Quito and Guadalupe fake_provider simulators, respectively, to demonstrate the comparison between the LCNNS method and mainstream compilers. The test data for this benchmark circuit is presented in Table I and Table II. And the corresponding data comparison graph is shown in Figs. 15-16. It is worth noting that four different methods are compared for synthesizing the CNOT circuit, namely Qiskit, Tket, HA and LCNNS. Qiskit is a quantum computing framework developed by IBM that can be used to build and simulate quantum circuits. Tket is a quantum compiler developed by Cambridge Quantum Computing that converts advanced quantum algorithms into quantum circuits. HA is a compilation method proposed in [30]. In the first three compilers, the default mapping strategy is selected for comparison. In terms of fidelity, the fidelity of the circuits in Tables I and II is optimized up to 5.7 times and 243.4 times on average.

In the NISQ era of quantum computing, one significant source of noise is the CNOT gate. Thus, reducing the number of CNOT gates during the synthesis process is instrumental in enhancing fidelity. The theoretical upper bound for the number of CNOT gates in an NN synthesized CNOT circuit has been established as $2n^2$, n represents the number of qubits in the circuit, as demonstrated in [28]. Tables I and II show that the number of CNOT gates under the LCNNS method is consistently below this upper bound, indirectly validating the theoretical correctness. In this study, noise factors are explicitly considered during the synthesis process, which further aids in improving the fidelity of the circuits. Therefore, the optimization rates presented in Tables I and II are considered in the context of this fidelity enhancement.

3. Synthesis on the BV algorithm

In order to extend the CNOT circuit synthesis method to overcome its limitation of being applicable only to CNOT circuits, the Bernstein-Vazirani quantum algorithm is used as an example to illustrate the extensibility of the CNOT circuit synthesis method. Bernstein-Vazirani is a quantum algorithm containing some single-qubit gates and CNOT gates, where the CNOT gates are continuous, as shown in Fig. 13. We synthesize this part of the CNOT circuits by using the LCNNS method, after adding the single-qubit gates into the synthesized circuits, making them equivalent to the original circuits. This method is tested on different types of architectures, which are shown in Table III, containing 1-D, grid, and 2-D, as well as architectures with or without Hamiltonian paths. Detailed parameters of these architectures are given in Appendices A and B. The demonstration results, as depicted in Fig. 14, demonstrate that the LCNNS approach is applicable to a variety of architectures

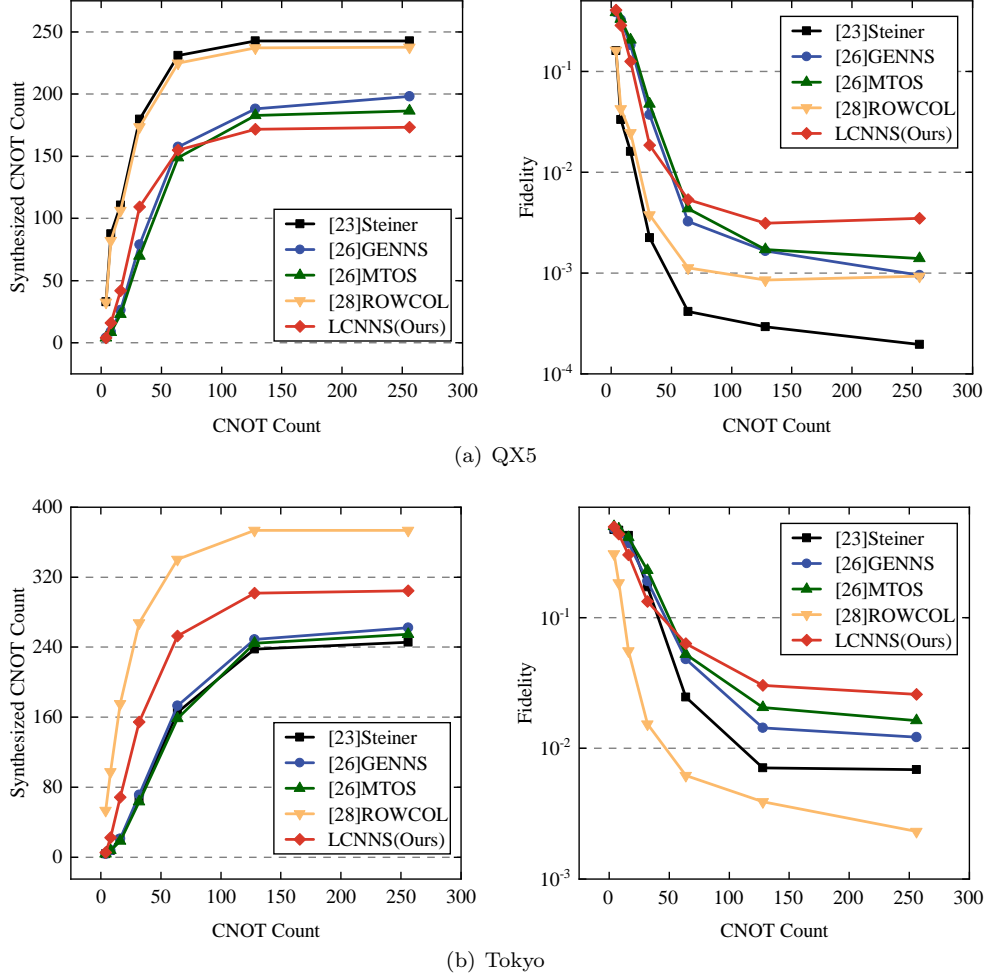


FIG. 12. Comparison of synthesized CNOT count and fidelity on IBMQ QX5 and Tokyo.

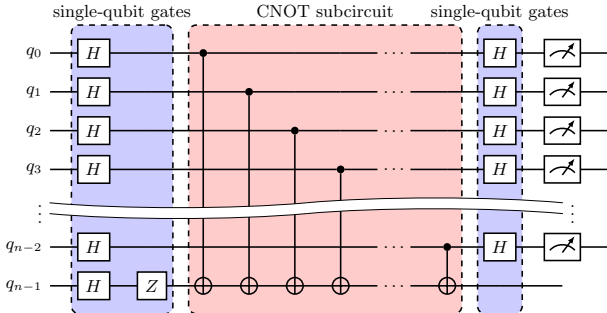


FIG. 13. Quantum circuit representation of the Bernstein-Vazirani algorithm. Inside the blue box are single-qubit gates, which are not subject to the NN constraints of the quantum architecture. In the red box are CNOT gates, and the NN of the whole circuit can be achieved by simply applying the LCNNS method to this portion of consecutive CNOT gates and then recombining them with the single-qubit gates.

under NISQ, and the average fidelity optimization rate is 14.85%. Furthermore, its applicability extends to circuits including single-qubit gates, such as Deutsch-Jozsa

circuits, QFT circuits.

C. Data analysis

1. CNOT count analysis

The number of CNOT gates is a critical metric for assessing the complexity of a CNOT quantum circuit, and it has a significant impact on the efficiency and reliability of quantum computing. A higher number of CNOT gates indicates more complex interactions between qubits, leading to longer execution times and higher error rates. Therefore, reducing the number of CNOT gates after circuit transformation is essential for achieving efficient quantum computing. In contrast to the traditional way of inserting SWAP gates to achieve the NN of quantum gates, this paper achieves the NN synthesis of CNOT circuits by means of matrix transformation. This method enables the NN constraint of each gate in a CNOT circuit without inserting additional SWAP gates. As a result, it effectively reduces the num-

TABLE I. The test data of 5-qubit random CNOT circuits on IBMQ_Quito's fake-provider simulator in Qiskit provided by the IBMQ cloud platform.

Circuit ^a	Qiskit			Tket			HA			LCNNS			Imp ^b
	CNOT ^c	Depth ^c	Fidelity ^c	CNOT	Depth	Fidelity	CNOT	Depth	Fidelity	CNOT	Depth	Fidelity	
5_10	19	16	0.6045	19	23	0.6025	23	21	0.5586	14	15	0.6670	1.10
5_20	35	26	0.4971	37	37	0.3584	46	39	0.3486	14	14	0.6543	1.32
5_30	69	61	0.1914	62	55	0.2217	68	61	0.2383	16	15	0.6162	2.59
5_40	75	66	0.2217	72	86	0.2129	100	83	0.1582	12	13	0.6855	3.09
5_50	115	97	0.1113	103	110	0.1152	110	89	0.1406	16	16	0.6357	4.52
5_100	225	196	0.0596	195	188	0.0557	209	176	0.0645	25	24	0.5049	7.83
5_200	492	441	0.0635	430	444	0.0625	482	404	0.0723	21	20	0.5205	7.20
5_500	1072	966	0.0625	977	986	0.0605	1094	919	0.0566	11	11	0.7197	11.52
5_1000	2296	2041	0.0723	2028	2123	0.0635	2436	2023	0.0547	28	26	0.4717	6.53
5_2000	4565	4033	0.0498	4042	4177	0.0576	4740	3923	0.0566	20	19	0.5479	9.51
5_5000	11547	10249	0.0635	10029	10314	0.0654	11984	9926	0.0645	20	19	0.5459	8.34
5_10000	23023	20529	0.0723	20047	20713	0.0566	23480	19592	0.0557	22	21	0.5479	7.58

^a The number 5 indicates 5 qubits, and the following number represents the number of CNOT gates, ranging from 10 to 10000.

^b Imp: the Imp is calculated as the ratio of the fidelity achieved using LCNNS to the highest fidelity among other methods. A ratio greater than 1 indicates optimization, with a larger ratio signifying more significant improvement.

^c CNOT, Depth, Fidelity: the number of CNOT gates, the depth of the circuit, and the circuit fidelity following compilation using four different methods: Qiskit, Tket, HA, and LCNNS.

ber of CNOT gates in the circuit after the NN synthesis. Compared with Qiskit and HA, Tket further decomposes the CNOT gate and other gates into single-qubit gates after the neighbors. So the number of CNOT gates in the Tket method is smaller than Qiskit and HA. As shown in Figs. 15(a) and 16(a), compared with the four NN methods and initial CNOT gates, the number of CNOT gates of the proposed LCNNS method is lower, and the average optimization rate of the number of CNOT gates reaches 39.1%. Furthermore, the LCNNS method takes architecture connectivity into account during the initial mapping process, which results in fewer synthesized CNOT gates in most circuits compared with the synthesis methods of the comparison models, as shown in Fig. 12. This advantage becomes even more pronounced in circuits with a higher gate count.

2. Depth analysis

Similar to the number of CNOT gates, the depth of a CNOT quantum circuit is also an important indicator of the complexity and reliability of the CNOT quantum circuit. The depth of a CNOT quantum circuit refers to the number of layers of CNOT gates in the CNOT quantum circuit. Figs. 15(b) and 16(b) show the comparison between the three methods and the LCNNS method in terms of circuit depth. From Figs. 15(b) and 16(b), it can be seen that the circuit depth of the LCNNS method is

much lower than those of the Qiskit, Tket and HA methods, with an average optimization rate of 20.5%. This is due to the significant effect of reducing the number of CNOT gates in the LCNNS method compared with other compiler methods.

3. Fidelity analysis

The fidelity of a quantum circuit refers to the degree of similarity between the output result of the circuit and the desired result, which can reflect the accuracy and reliability of the circuit. In quantum computing, it is essential that the output result of a quantum circuit is as close as possible to the desired result, so fidelity is one of the most important indicators of the performance of a quantum circuit. Figs. 15(c) and 16(c) present a comparison between the Qiskit, Tket, HA and our LCNNS method in terms of circuit fidelity. It can be seen that the proposed LCNNS method greatly outperforms other methods in optimizing the circuit execution fidelity. Similarly, once the number of CNOT gates reaches a certain size, the fidelity of LCNNS synthesized circuits exceeds that of other synthesis methods, as shown in Fig. 12. There are two reasons for this. On the one hand, the CNOT circuit synthesis method achieves quantum gates that satisfy the NN constraint with as few CNOT gates as possible, and reducing the number of CNOT gates similarly reduces the source of double quantum gate errors, thus improv-

TABLE II. The test data of 16-qubit random CNOT circuits on the IBMQ_Guadalupe's fake_provider simulator in Qiskit provided by the IBMQ cloud platform.

Circuit	Qiskit				Tket				HA				LCNNS				Imp
	CNOT	Depth	Fidelity	CNOT	Depth	Fidelity	CNOT	Depth	Fidelity	CNOT	Depth	Fidelity	CNOT	Depth	Fidelity		
16_10	26	15	0.7842	31	19	0.7510	62	28	0.6594	125	87	0.4463	125	87	0.4463	0.57	
16_20	61	30	0.6611	60	44	0.6543	129	56	0.5251	148	86	0.4492	148	86	0.4492	0.68	
16_30	105	40	0.5508	105	55	0.5576	156	68	0.4756	210	135	0.3369	210	135	0.3369	0.60	
16_40	151	69	0.3992	173	90	0.4199	224	113	0.3389	210	130	0.3115	210	130	0.3115	0.74	
16_50	240	96	0.2815	293	147	0.2168	374	164	0.2009	258	149	0.2461	258	149	0.2461	0.87	
16_100	475	198	0.1033	576	307	0.0596	651	319	0.0635	242	129	0.2568	242	129	0.2568	2.49	
16_200	1043	425	0.0061	1261	692	0.0029	1535	697	0.0037	272	158	0.2246	272	158	0.2246	36.80	
16_500	2751	1056	0.0002	3115	1660	0.0002	3733	1654	0.0001	250	141	0.2627	250	141	0.2627	1076.00	
16_1000	5634	2208	0.0001	6091	3172	0.0010	7743	3660	0.0001	259	137	0.2422	259	137	0.2422	248.00	
16_2000	11374	4633	0.0002	12116	6452	0.0005	15236	6997	0.0002	254	137	0.2383	254	137	0.2383	488.00	
16_5000	29184	11545	0.0002	31231	16807	0.0002	38507	18106	0.0002	247	133	0.2637	247	133	0.2637	1080.00	
16_10000	58942	23212	0.0003	63282	33848	0.0003	77780	35606	0.0002	282	159	0.2422	282	159	0.2422	793.60	

* The notes in Table II are consistent with Table I.

TABLE III. Parameters for different types of Architectures.

Architecture	Makers	Qubit	Layout	Hamiltonian paths
Wuyuan II ^a	Origin	6	1-D	YES
Wukong ^a	Origin	12	2-D	NO
ScQ-10 ^a	Quafu	10	1-D	YES
ScQ-18 ^a	Quafu	18	1-D	YES
Manila ^b	IBMQ	5	1-D	YES
Quito ^b	IBMQ	5	2-D	NO
Jakarta ^b	IBMQ	7	2-D	NO
Guadalupe ^b	IBMQ	16	2-D	NO
Tokyo ^b	IBMQ	20	Grid	YES
Almaden ^b	IBMQ	20	Grid	NO
Kolkata ^b	IBMQ	27	2-D	NO

^a These QPUs are provided by the OriginQ Quantum Cloud Platform and the Quafu Cloud Platform in China, respectively.

^b These QPUs are provided by the IBMQ Cloud Platform.

ing the fidelity of the synthesized CNOT circuit. On the other hand, the fidelity of CNOT gates is taken into account for the initial mapping, and the CNOT gates are prioritized to act on the path with a lower error rate during the matrix transformation. The trade-off between the number of CNOT gates and the fidelity of the simulation is chosen to achieve the CNOT circuit synthesis at a lower cost. This also explains why, in certain circuits as shown in Fig. 12b, the LCNNS method achieves the

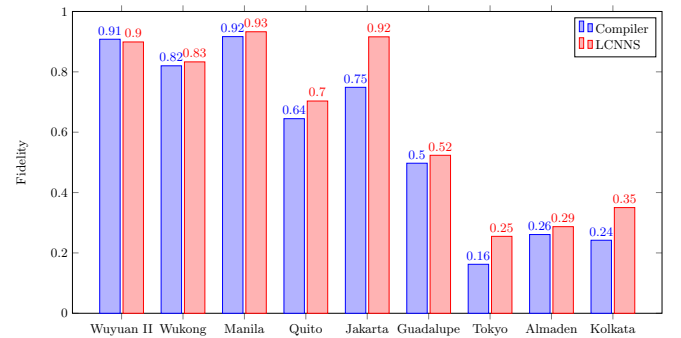


FIG. 14. Comparison of the fidelity of the Bernstein-Vazirani algorithm for each architecture in Table III. The fidelity calculation method is ESP. The circuits demonstrated on the Origin and Quafu platforms are executed on the actual devices. Since the fidelity of the compiler execution on the Quafu platform is 0.0195 and 0.0008, respectively, and 0.326 and 0.011 for LCNNS, respectively, the data are too small to be presented in Fig 14. And the circuits demonstrated on the IBMQ platform are executed on the fake_provider simulator. This observation demonstrates the versatility of the LCNNS method, as it applies effectively to various architectural configurations, including 1-D, 2-D, and grid architectures, both with and without Hamiltonian paths. Notably, the LCNNS method exhibits superior fidelity performance compared with alternative methods.

highest fidelity compared with other synthesis methods, even though it has more CNOT gates than the others. Therefore, in terms of fidelity, the LCNNS method is more suitable for circuits with a high number of CNOT gates.

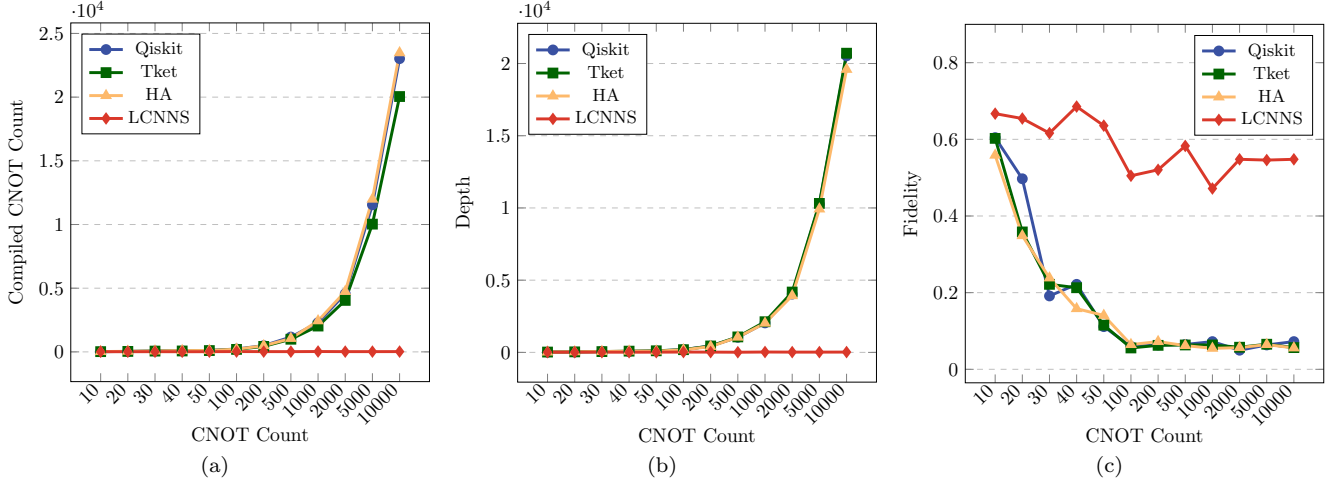


FIG. 15. Comparison of results in Table I under three performance indicators. (a) Comparison of CNOT gate numbers: As the number of CNOT gates increases, the number of CNOT gates in the circuits after the NN of the comparison methods tends to increase. The LCNNS method stands out by maintaining a significantly lower count of CNOT gates compared to other methods. (b) Comparison of depth: Similar to (a), the aspect of circuit depth follows the same trend, with LCNNS consistently achieving shallower circuit depth than other methods. (c) Comparison of fidelity: The increase in the number of CNOT gates results in a noticeable decrease in fidelity in circuits after applying the NN methods of comparison. However, the LCNNS method demonstrates the capability to maintain high fidelity even with an increased number of CNOT gates.

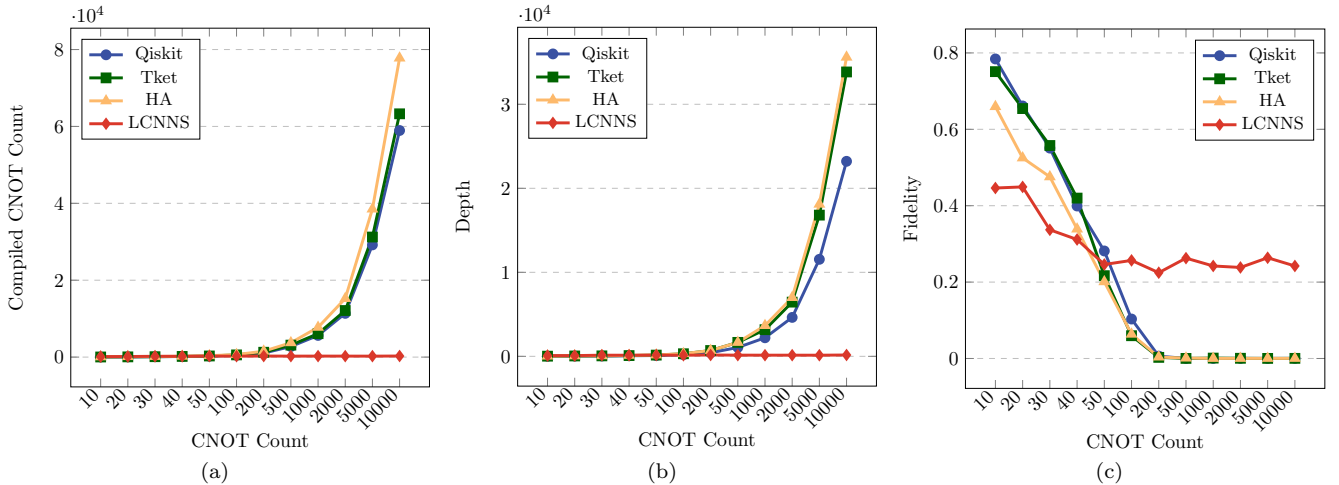


FIG. 16. Comparison of circuits in Table II under three performance indicators. (a) Comparison of CNOT gate numbers: When the circuit size is large, the LCNNS method still keeps the number of CNOT gates at a low level, while the number of CNOT gates after NN of the comparison method grows linearly with the size. (b) Comparison of depth: The increase in the number of CNOT gates similarly leads to an increase in depth, which maintains essentially the same rate of increase in (a). (c) Comparison of fidelity: The fidelity of the comparison methods tends towards 0, but the fidelity of LCNNS overwhelmingly still manages to be greater than the 0.5 threshold.

VI. DISCUSSION

The method presented in this paper exhibits applicability across various IBM quantum computer architectures, especially those without Hamiltonian paths. Consequently, it can be effectively employed on a diverse range of quantum computing platforms in the NISQ. It is worth emphasizing that the suggested approach ex-

tends its utility to quantum circuits that incorporate not only pure CNOT gates but also additional single-qubit gates, such as Clifford+T circuits. This versatility arises from the capability of reassembling a quantum circuit containing CNOT subcircuits into a form that satisfies the NN constraint. This is achieved by synthesizing the CNOT subcircuits and subsequently reassembling the circuit with single-qubit gates.

The performance of the proposed method for compiling Clifford+T gate set circuits under varying CNOT gate ratios is evaluated. Randomly generated 5-qubit quantum circuits are used, with gate counts (including both single-qubit and CNOT gates) ranging from 20 to 10,000, and the CNOT gate ratio in the circuits is set to range from 10% to 100%. In comparison to the Qiskit method, the number of CNOT gates is selected as the performance metric, and demonstrations are conducted on the IBMQ_Quito simulator, with the results presented in Fig. 17.

From the results shown in Fig. 17, it can be observed that with the increase in the CNOT gate ratio, the number of CNOT gates in the Qiskit method exhibits an upward trend, whereas the number of CNOT gates in the LCNNS method initially increases and then decreases. Intersection points in the CNOT gate counts between the two methods occur at certain ratios. This indicates that the LCNNS method is more suitable for handling circuits with a higher number of CNOT gates. As the CNOT gate ratio increases, the advantage of the LCNNS method becomes more apparent, with the number of CNOT gates showing an initial increase followed by a decrease. Therefore, when the CNOT gate ratio reaches a certain threshold, the optimization effect of the LCNNS method surpasses that of the Qiskit method.

To further investigate the CNOT gate ratio threshold at which the LCNNS method outperforms the Qiskit method for different numbers of qubits, tests are conducted on 5-qubit, 7-qubit, 14-qubit, 16-qubit, and 20-qubit circuits, each with 1,000 gates. The demonstrations of these circuits were conducted on IBMQ_Quito, BMQ_Jakarta, BMQ_Melbourne, BMQ_Guadalupe, and BMQ_Almaden simulators, respectively. The results, shown in Fig. 18, indicate that as the number of qubits increases, the threshold at which the LCNNS method outperforms the Qiskit method gradually approaches 100%. It is important to note that Fig. 18 only shows the threshold for circuits with 1,000 gates, and the thresholds may differ for circuits with different gate counts. This phenomenon provides substantial insights for quantum circuit compilation: when the number of CNOT gates in a circuit is low or below a certain threshold, the insertion of SWAP gates to achieve nearest-neighbor compliance may be employed; conversely, when the number of CNOT gates is high or exceeds a certain threshold, utilizing the nearest-neighbor synthesis for CNOT gates might be more beneficial.

In summary, this section reveals the significant advantages of the LCNNS method in handling quantum circuits with high CNOT gate ratios and provides new optimization strategies for quantum circuit compilation. As the CNOT gate ratio increases, the LCNNS method demonstrates stronger optimization capabilities, making it a preferable choice over the traditional Qiskit method under certain conditions. The implication is that CNOT circuits generated using this method can be easily scaled to more complex quantum circuits, substantially enhanc-

ing the fidelity of CNOT circuits post-synthesis and execution. This enhancement is of paramount significance for the practical deployment of CNOT circuits in various quantum computing contexts. Future work could explore optimization strategies for quantum circuits of different scales and structures, further enhancing quantum circuit compilation techniques.

VII. CONCLUSION

This work presents an effective approach to synthesizing CNOT quantum circuits on general quantum computing devices with and without Hamiltonian paths. Specifically, the proposed key-qubit priority model and tabu search algorithm are employed to dynamically adjust the mapping method of key qubits, with the aim of reducing the number of CNOT gates and increasing circuit fidelity after matrix transformation. Additionally, a noise-aware NN synthesis method based on layer convergence is presented. These approaches effectively improve the fidelity of the synthesized circuit, providing a new solution to the problem of synthesizing CNOT circuits on real quantum computing devices. The demonstration results, performed on the IBMQ_Quito quantum architecture and other architectures in the cloud platform, demonstrate that the proposed method can significantly enhance the execution fidelity of CNOT quantum circuits on real quantum hardware. While these methods enhance fidelity significantly, it is crucial to note that the complexity of synthesizing circuits increases factorially with the number of qubits, posing scalability challenges. Future work will focus on developing more efficient synthesis techniques to address this complexity and extend our methods to more complex quantum circuits.

ACKNOWLEDGMENT

The work was supported by the National Natural Science Foundation of China under Grant number 62072259, in part by the Natural Science Foundation of Jiangsu Province under Grant number BK20221411, in part by the Natural Science Foundation of Nantong under Grant number JC2024100, in part by the PhD Start-up Fund of Nantong University under Grant number 23B03, in part by the Postgraduate Research and Practice Innovation Program of Jiangsu Province under Grant number SJCX21_1448 and SJCX23_1782.

DATA AND CODE AVAILABILITY

The raw test data of this study and the software codes for generating the test data are publicly available at <https://github.com/M-qiangZhu/Nearest-neighbor-synthesis-of-CNOT-circuits-on-general-quantum-architectures>.

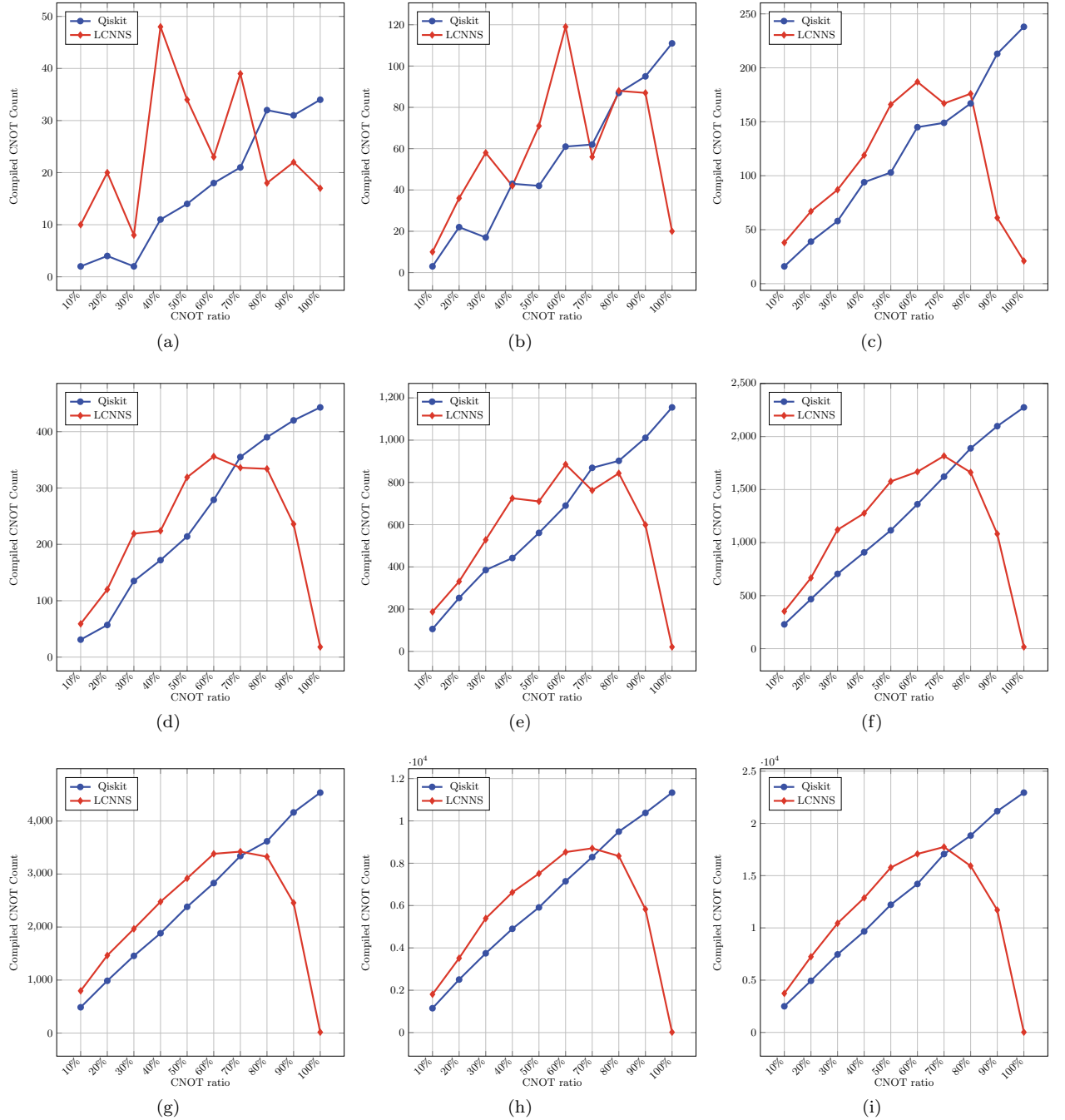


FIG. 17. Comparison of the number of CNOT gates between Qiskit and LCNNS methods under different CNOT gate ratios for various total circuit gate scales: (a)-(i) corresponding to 20, 50, 100, 200, 500, 1000, 2000, 5000, 10000 gates.

- [1] X. Peng, Z. Liao, N. Xu, G. Qin, X. Zhou, D. Suter, and J. Du, Quantum adiabatic algorithm for factorization and its experimental implementation, *Physical review letters* **101**, 220405 (2008).
- [2] S. Jujiang, K. A. Britt, A. J. McCaskey, T. S. Humble, and S. Kais, Quantum annealing for prime factorization, *Scientific reports* **8**, 17667 (2018).

- [3] P. R. Giri and V. E. Korepin, A review on quantum search algorithms, *Quantum Information Processing* **16**, 1 (2017).
- [4] S. Somaroo, C. Tseng, T. Havel, R. Laflamme, and D. G. Cory, Quantum simulations on a quantum computer, *Physical review letters* **82**, 5381 (1999).

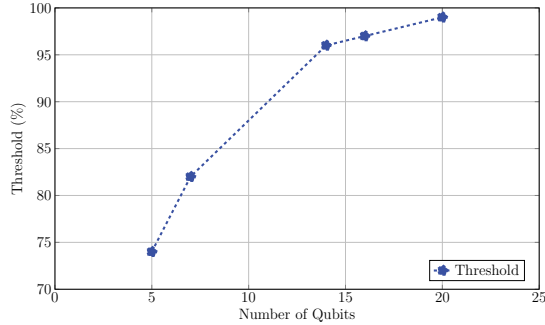


FIG. 18. Relationship between the number of qubits and threshold. The threshold means that when the ratio of CNOT gates in the circuit is greater than this value, the LCNNS method will outperform Qiskit.

[5] A. Kumar and S. Garhwal, State-of-the-art survey of quantum cryptography, *Archives of Computational Methods in Engineering* **28**, 3831 (2021).

[6] H.-J. Werner, P. J. Knowles, G. Knizia, F. R. Manby, and M. Schütz, Molpro: a general-purpose quantum chemistry program package, *Wiley Interdisciplinary Reviews: Computational Molecular Science* **2**, 242 (2012).

[7] S. McArdle, S. Endo, A. Aspuru-Guzik, S. C. Benjamin, and X. Yuan, Quantum computational chemistry, *Reviews of Modern Physics* **92**, 015003 (2020).

[8] V. Dunjko and H. J. Briegel, Machine learning & artificial intelligence in the quantum domain: a review of recent progress, *Reports on Progress in Physics* **81**, 074001 (2018).

[9] H. Situ, Z. He, Y. Wang, L. Li, and S. Zheng, Quantum generative adversarial network for generating discrete distribution, *Information Sciences* **538**, 193 (2020).

[10] A. Barenco, C. H. Bennett, R. Cleve, D. P. DiVincenzo, N. Margolus, P. Shor, T. Sleator, J. A. Smolin, and H. Weinfurter, Elementary gates for quantum computation, *Physical review A* **52**, 3457 (1995).

[11] P. Zhu, X. Cheng, and Z. Guan, An exact qubit allocation approach for nisq architectures, *Quantum Information Processing* **19**, 391 (2020).

[12] X. Cheng, Z. Guan, and P. Zhu, Nearest neighbor transformation of quantum circuits in 2d architecture, *IEEE Access* **8**, 222466 (2020).

[13] P. Zhu, W. Ding, L. Wei, X. Cheng, Z. Guan, and S. Feng, A variation-aware quantum circuit mapping approach based on multi-agent cooperation, *IEEE Transactions on Computers* (2023).

[14] B. Nash, V. Gheorghiu, and M. Mosca, Quantum circuit optimizations for nisq architectures, *Quantum Science and Technology* **5**, 025010 (2020).

[15] M. Amy, P. Azimzadeh, and M. Mosca, On the controlled-not complexity of controlled-not-phase circuits, *Quantum Science and Technology* **4**, 015002 (2018).

[16] S. Zhang, J. Wu, and L. Li, Characterization, synthesis, and optimization of quantum circuits over multiple-control z-rotation gates: A systematic study, *Physical Review A* **108**, 022603 (2023).

[17] X. Cheng, M. Zhu, X. Li, and Z. Guan, Nearest neighbor synthesis of cnot circuit based on matrix transformation, in *Advances in Natural Computation, Fuzzy Systems and Knowledge Discovery: Proceedings of the ICNC-FSKD 2021* **17** (Springer, 2022) pp. 150–156.

[18] S. Zhang, K. Huang, and L. Li, Automatic depth-optimized quantum circuit synthesis for diagonal unitary matrices with asymptotically optimal gate count, *arXiv preprint arXiv:2212.01002* (2022).

[19] V. Gheorghiu, J. Huang, S. M. Li, M. Mosca, and P. Mukhopadhyay, Reducing the cnot count for clifford+ t circuits on nisq architectures, *IEEE Transactions on Computer-Aided Design of Integrated Circuits and Systems* (2022).

[20] K. Markov, I. Patel, and J. Hayes, Optimal synthesis of linear reversible circuits, *Quantum Information and Computation* **8**, 0282 (2008).

[21] B. Schaeffer and M. Perkowski, Linear reversible circuit synthesis in the linear nearest-neighbor model, in *2012 IEEE 42nd International Symposium on Multiple-Valued Logic* (IEEE, 2012) pp. 157–160.

[22] T. G. De Brugiére, M. Baboulin, B. Valiron, S. Martiel, and C. Allouche, Gaussian elimination versus greedy methods for the synthesis of linear reversible circuits, *ACM Transactions on Quantum Computing* **2**, 1 (2021).

[23] A. Kissinger and A. Meijer-van de Griend, Cnot circuit extraction for topologically-constrained quantum memories, *Quantum Information and Computation* **20**, 581 (2020).

[24] T. G. de Brugiére, M. Baboulin, B. Valiron, S. Martiel, and C. Allouche, Quantum cnot circuits synthesis for nisq architectures using the syndrome decoding problem, in *Reversible Computation: 12th International Conference, RC 2020, Oslo, Norway, July 9–10, 2020, Proceedings* **12** (Springer, 2020) pp. 189–205.

[25] A. Meijer-van de Griend and S. M. Li, Dynamic qubit allocation and routing for constrained topologies by cnot circuit re-synthesis, in *Quantum Physics and Logic* (Electronic Proceedings in Theoretical Computer Science, 2022).

[26] M. Zhu, X. Cheng, P. Zhu, L. Chen, and Z. Guan, Physical constraint-aware cnot quantum circuit synthesis and optimization, *Quantum Information Processing* **22**, 10 (2022).

[27] C. Chen, B. Schmitt, H. Zhang, L. S. Bishop, and A. Javadi-Abhari, Recursive methods for synthesizing permutations on limited-connectivity quantum computers, *arXiv preprint arXiv:2207.06199* (2022).

[28] B. Wu, X. He, S. Yang, L. Shou, G. Tian, J. Zhang, and X. Sun, Optimization of cnot circuits on limited-connectivity architecture, *Physical Review Research* **5**, 013065 (2023).

[29] C.-K. Li, R. Roberts, and X. Yin, Decomposition of unitary matrices and quantum gates, *International Journal of Quantum Information* **11**, 1350015 (2013).

[30] S. Niu, A. Suau, G. Staffelbach, and A. Todri-Sanial, A hardware-aware heuristic for the qubit mapping problem in the nisq era, *IEEE Transactions on Quantum Engineering* **1**, 1 (2020).

[31] S. B. Nadler Jr, Continuum theory and graph theory: disconnection numbers, *Journal of the London Mathematical Society* **2**, 167 (1993).

[32] F. Glover, E. Taillard, and E. Taillard, A user's guide to tabu search, *Annals of operations research* **41**, 1 (1993).

[33] U. Brandes, A faster algorithm for betweenness centrality, *Journal of mathematical sociology* **25**, 163 (2001).

- [34] R. M. Karp, *Reducibility among combinatorial problems* (Springer, 2010).
- [35] R. Wille, D. Große, L. Teuber, G. W. Dueck, and R. Drechsler, Revlib: An online resource for reversible functions and reversible circuits, in *38th International Symposium on Multiple Valued Logic (ismvl 2008)* (IEEE, 2008) pp. 220–225.
- [36] OriginQ, Origin quantum, Website (2023), <https://qcloud.originqc.com.cn/zh/computerServices/services>.
- [37] B. I. of Quantum Information Science, Quafu, Website (2023), <https://quafu.baqis.ac.cn/>.
- [38] IBM, Ibm quantum compute resources, Website (2023), <https://quantum-computing.ibm.com/services/resources?tab=systems>.
- [39] qiskit, Fake provider, Website (2023), https://qiskit.org/documentation/apidoc/providers_fake_provider.html.

Appendix A: Coupling graphs

In this Appendix, we show various architectures on different quantum cloud platforms. These platforms include the OriginQ Quantum Cloud Platform [36] in China, the Cloud Platform of Beijing Institute of Quantum Information Science [37] in China, and the IBMQ Cloud Platform.

OriginQ Quantum Cloud Platform is launched by OriginQ Quantum Computing Technology (Hefei) Co. It provides real quantum computing, quantum computing simulators, and super-quantum hybrid computing backend access. It provides basic software and development tools for developers, and industry application services for advanced companies in biochemistry, financial technology, big data, and machine learning. Users can access the following link, <https://qcloud.originqc.com.cn/zh/home>. The coupling graph of the quantum computing device provided by OriginQ is shown in Fig. 19.

Quafu is a quantum computing cloud platform launched by Beijing Institute of Quantum Information Science in collaboration with Institute of Physics, Chinese Academy of Sciences and Tsinghua University, with the meaning of "quantum future". At present, there are three superconducting quantum chips on the platform, which have 136, 18 and 10 qubits, respectively, and users can independently choose the appropriate chip to run quantum computing tasks. Users can access the following link, <https://quafu.baqis.ac.cn>. The coupling graph of the quantum computing device provided by Quafu is shown in Fig. 20.

IBM Quantum Platform is a cloud-based quantum computing service provided by IBM that allows users to access and explore quantum computing over the Internet. It provides quantum computer hardware, the Qiskit programming framework, and a wealth of educational resources to provide researchers and developers with easy access to quantum computing resources and tools. IBMQ supports the development of quantum computing

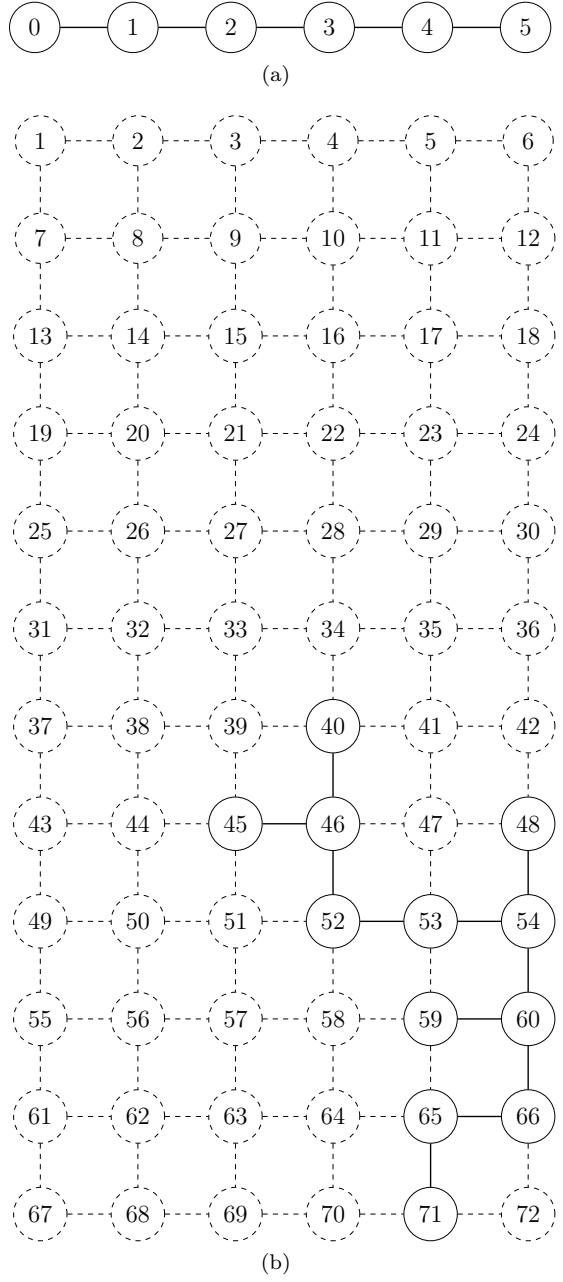
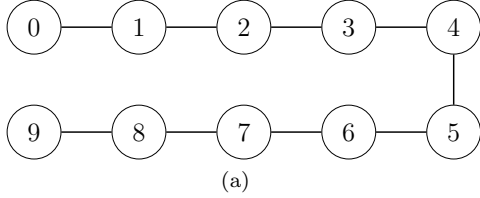
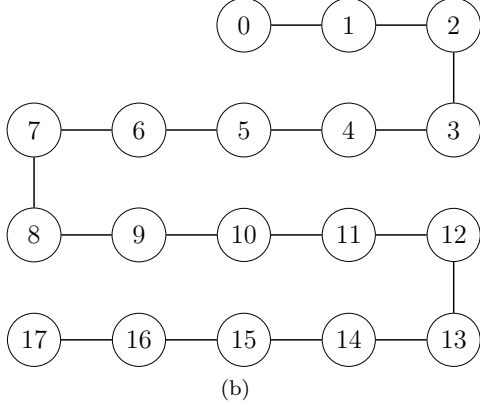


FIG. 19. (a) The coupling graph of Wuyuan II. (b) The coupling graph of Wukong. The dashed qubits and connecting lines indicate unavailable qubits and couplings. Therefore, the number of qubits currently available for this QPU is 12.

research and applications through open cloud services. Users can access the following link, <https://quantum-computing.ibm.com>. In addition to the architecture shown in Fig. 2, the coupling graph of IBMQ's quantum computing devices used in the demonstration is shown in Fig. 21.



(a)



(b)

FIG. 20. (a) and (b) are the coupling graphs of the QPUs of the Quafu cloud platform at 10 and 18 qubits, respectively, and both are 1-D architectures.

TABLE IV. Calibration data for Fig. 2(a), IBMQ_quito.

Qubit1	Qubit2	CNOT error
Q0	Q1	1.63E-02
Q1	Q2	7.77E-03
Q1	Q3	7.44E-03
Q3	Q4	8.79E-03

Appendix B: Parameter metrics

In this Appendix, we show the specific parameter metrics of the devices of each quantum computing cloud platform, such as T1, T2, error rate, etc. And each platform offers different parameters. It is important to note that these parameters change with calibration, so the specific values of these metrics are based on the time of the circuit demonstration. Tables IV to VIII show the detailed parameters of the real devices, each table corresponding to an architecture. Table IX provides only the average parameter metrics for the fake-provider simulator on the IBMQ cloud platform.

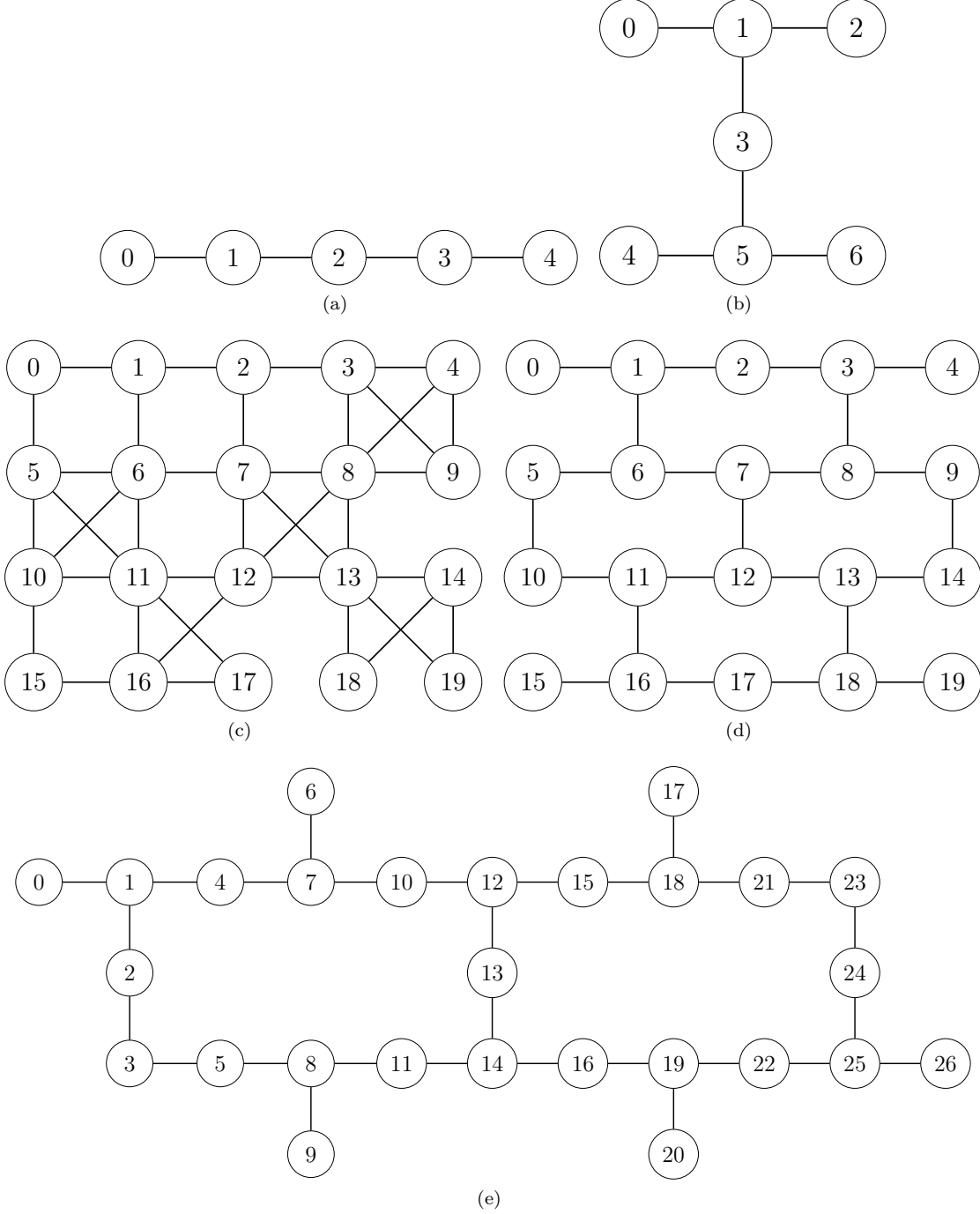


FIG. 21. (a)-(e) Manila, Jakarta, Tokyo, Almaden, and Kolkatta of the IBMQ cloud platform, respectively.

TABLE V. Calibration data for Wuyuan II of OriginQ cloud platform in China.

Qubit	T1(μ s)	T2(μ s)	Readout fidelity(F0/F1)	Single-qubit gate fidelity	Connection	CZ fidelity
Q0	12	2.7	0.971/0.897	0.9989	Q0-Q1	0.9851
Q1	22	9.3	0.922/0.801	0.9989	Q1-Q2	0.9619
Q2	4	7.1	0.978/0.883	0.9961	Q2-Q3	0.7014
Q3	14	17.8	0.960/0.885	0.998	Q3-Q4	0.8256
Q4	9	10.3	0.968/0.901	0.9987	Q4-Q5	0.7132
Q5	16	3.3	0.944/0.868	0.9982	—	—

TABLE VI. Calibration data for Wukong of OriginQ cloud platform in China.

Qubit	T1(μ s)	T2(μ s)	Readout fidelity(F0/F1)	Single-qubit gate fidelity	Connection	CZ fidelity
Q40	26.007	0.532	0.8997	0.9973	Q40_Q46	0.8813
Q45	26.58	0.354	0.8844	0.9905	Q45_Q46	0.9744
Q46	23.758	0.707	0.8948	0.998	Q46_Q52	0.97
Q48	13.582	0.339	0.8629	0.9963	Q48_Q54	0.9637
Q52	19.289	0.977	0.929	0.9986	Q52_Q53	0.9714
Q53	31.361	0.63	0.9454	0.9946	Q53_Q54	0.978
Q54	22.699	5.941	0.863	0.9986	Q54_Q60	0.9721
Q59	11.857	5.694	0.8859	0.9955	Q59_Q60	0.9636
Q60	14.697	4.454	0.8798	0.9972	Q60_Q66	0.9709
Q65	20	10	0.9175	0.9974	Q65_Q71	0.9613
Q66	20	10	0.8695	0.9964	—	—
Q71	20	10	0.8806	0.9975	—	—

TABLE VII. Calibration data for ScQ-10 of Quafu cloud platform in China.

Qubit	T1(μ s)	T2(μ s)	Anharmonicity(GHZ)	Qubit frequency(GHZ)	Readout frequency(GHZ)	Connection	CZ fidelity
Q1	26.79	2.33	0.25	5.31	6.6636	Q2_Q1	0.9787
Q2	29.38	1.82	0.207	4.681	6.6461	Q3_Q2	0.9564
Q3	58.96	2.31	0.246	5.367	6.6277	Q4_Q3	0.949
Q4	18.92	1.61	0.206	4.702	6.608	Q5_Q4	0.963
Q5	43.38	2.49	0.250682	5.299	6.5933	Q6_Q5	0.9669
Q6	47.37	2.14	0.203	4.531	6.5706	Q7_Q6	0.9663
Q7	37.88	1.97	0.2515	5.255	6.5541	Q8_Q7	0.956
Q8	19.5	1.33	0.2035	4.627	6.5318	Q9_Q8	0.9741
Q9	31.51	1.72	0.2462	5.275	6.5109	Q9_Q10	0.9909
Q10	23.43	3.56	0.208	4.687	6.4905	—	—

TABLE VIII. Calibration data for ScQ-18 of Quafu cloud platform in China.

Qubit	T1(μ s)	T2(μ s)	Anharmonicity(GHZ)	Qubit frequency(GHZ)	Readout frequency(GHZ)	Connection	CZ fidelity
Q3	57.56365654	4.239166288	0.204783115	4.59	6.77627	Q4_Q3	0.989946019
Q4	27.88541771	3.699022109	0.191726174	5.02	6.75915	Q5_Q4	0.921217382
Q5	41.44235979	4.83465697	0.2026145	4.62	6.73673	Q6_Q5	0.903526443
Q6	40.10235639	2.298777179	0.198	5.071	6.71278	Q7_Q6	0.927608543
Q7	28.9943269	5.690175203	0.204836532	4.5	6.69334	Q8_Q7	0.976533411
Q8	23.60180849	2.203347967	0.19367078	4.982	6.675695	Q9_Q8	0.805179376
Q9	26.83896243	3.419803923	0.203920589	4.566	6.649799022	Q9_Q10	0.969400313
Q10	19.75997688	2.437594747	0.2	5.091	6.6334	Q11_Q10	0.9825224
Q11	23.21915934	3.533866245	0.206	4.646	6.625063867	Q12_Q11	0.965295259
Q12	27.30825285	1.324619262	0.2	5.038	6.647559341	Q13_Q12	0.973640043
Q13	41.15484398	2.77881436	0.204648089	4.605	6.665	Q14_Q13	0.95548674
Q14	28.11873582	1.493925899	0.198	4.993	6.69280357	Q15_Q14	0.9514352
Q15	45.11682637	2.953474165	0.206	4.545	6.705075651	Q16_Q15	0.971210129
Q16	29.79524557	1.568231794	0.198	4.869	6.725190179	Q17_Q16	0.966539068
Q17	45.11688811	5.466767893	0.204114512	4.578	6.751021438	Q18_Q17	0.982567594
Q18	37.2792584	3.068254432	0.196	5.048	6.770705353	Q19_Q18	0.979586641
Q19	40.83724158	5.153026625	0.203098846	4.682	6.787665	Q20_Q19	0.984410078
Q20	41.42844931	3.116332126	0.196583622	5.125	6.807017363	—	—

TABLE IX. Calibration data for architectures on IBMQ cloud platform.

Architecture	T1(μs)	T2(μs)	Single-qubit gate error	CNOT error
Manila	0.1125	0.0372	0.0011	0.0116
Quito	0.0615	0.0518	0.0017	0.0354
Jakarta	0.1284	0.0339	0.0003	0.0126
Guadalupe	0.0702	0.0881	0.0004	0.0108
Tokyo	0.0876	0.0519	—	0.0313
Almaden	0.0868	0.0643	—	0.0238
Kolkata	0.1099	0.0968	0.0003	0.0109